3-25-2005

Effect of Fiber Volume Fraction on Fracture Mechanics in Continuously Reinforced Fiber Composite Materials

Thomas Wasik
University of South Florida

Effect of Fiber Volume Fraction on Fracture Mechanics in Continuously Reinforced Fiber Composite Materials

by

Thomas Wasik

A thesis submitted in partial fulfillment
of the requirements for the degree of
Master of Science in Mechanical Engineering
Department of Mechanical Engineering
College of Engineering
University of South Florida

Major Professor: Autar K. Kaw, Ph.D.
Glen H. Besterfield, Ph.D.
Thomas Eason, Ph.D.

Date of Approval:
March 25, 2005

Keywords: Finite Element, Crack Propagation, Composite Interface, Ansys, Interface Failure Modes

TABLE OF CONTENTS

LIST OF TABLES

LIST OF FIGURES

LIST OF SYMBOLS

E	Modulus of Elasticity
G, μ	Modulus of Rigidity
α	Coefficient of Thermal Expansion
V	Fiber Volume Fraction
ν	Poisson's ratio
K_I	Stress Intensity Factor
u	Displacement
ε	Strain
σ , τ	Stress
a	Crack Length
r	Radius
k	Plane-Strain Bulk Modulus
σ_1	Maximum Principle Stress
Γ	Energy Release Rate
p	Pressure
J_0	Bessel Function of zero order
b	Width of Fiber and Matrix

Subscripts

m	Matrix
f	Fiber
r, z, θ	Cylindrical Coordinates
d	Deflection
p	Penetration

c	Mode I Toughness
ic	Toughness of Interface
int	Interface
fib	Fiber
mat	Matrix

EFFECT OF FIBER VOLUME FRACTION ON FRACTURE MECHANICS IN CONTINUOUSLY REINFORCED FIBER COMPOSITE MATERIALS

Thomas Wasik

ABSTRACT

The application of advanced composite materials, such as graphite/epoxy, has been on the rise for the last four decades. The mechanical advantages, such as their higher specific stiffness and strength as compared to monolithic materials, make them attractive for aerospace and automotive applications. Despite these advantages, composites with brittle fibers have lower ductility and fracture toughness than monolithic materials.

One way to increase the fracture toughness of composites is to have a weak fiber-matrix interface that would blunt crack tips by crack deflection into the interface and hence enhance fracture toughness. However, this also reduces the transverse properties of the composite. Therefore, an optimum fiber-matrix interface would be the one that is just weak enough to cause crack deflection into interface.

This study investigates the effect of fiber-to-matrix moduli ratio, fiber-volume fraction, fiber orthotropy, and thermal stresses on the possibility of crack

deflection. A finite element model is used to analyze a 2-D axisymmetric representative volume element- a three-phase composite cylinder made of fiber, matrix, and composite. A penny shaped crack is assumed in the fiber.

To determine whether the crack would deflect into the interface or propagate into the matrix, maximum stresses at the fiber-matrix interface and in the matrix are compared to the interface and matrix strengths.

As opposed to most studies in the literature, this study found that fiber-volume fractions do have an impact on crack deflection and this impact increases with large fiber-to-matrix moduli ratios. The presence of orthotropic fiber in the composite increases the possibility of crack deflection with increasing fiber-volume fraction in the early and middle stages of the fiber crack growth. The thermal stresses decrease the likelihood of crack deflection when the thermal expansion coefficient of the matrix is larger than that of the fiber.

CHAPTER 1

INTRODUCTION

1.1 Overview

The use of composite materials has been steadily increasing in the past several decades. The high strength, high stiffness and lightweight make them particularly attractive to designers in a variety of industries. The composite material consists of a matrix and one of the reinforcing phases such as particulate, flake and fiber. In the continuous fiber composites, due to its large surface area, the fiber-matrix interface influences the behavior of a composite. In addition to providing a mechanism to transfer loads from matrix to fibers, the interface also plays an important role in determining the composite toughness.

In spite of many advantages, the composite materials suffer from lower ductility and toughness when compared to commonly used metals. A unidirectional composite with brittle fibers and a crack propagating perpendicular to the fibers can fail in at least three modes under longitudinal tensile load. These modes are:(a) brittle failure, (b) brittle failure with fiber pullout, (c) brittle failure with fiber pullout and interface shear failure or interface tensile failure [1]. This is illustrated in Figure 1. The tensile or shear interface failure is a prerequisite for phenomena such as crack deflection into the interface, crack bridging by fibers, and fiber pullout [2].

All of these are energy-dissipating phenomena during crack propagation process and help enhance toughness of the fiber-reinforced composites.

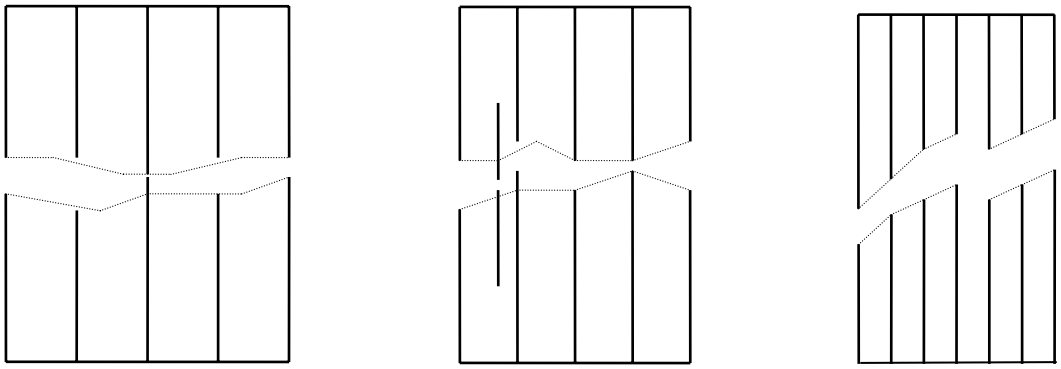

Figure 1: Modes of Failure of Unidirectional Lamina Under a Longitudinal Tensile Load

By controlling the strength of the interface bond between matrix and the fiber, the designer is able to influence the mechanical properties of the composite. To take a full advantage of the fiber properties and to obtain high strength and high stiffness composite, a strong fiber-matrix bond is very desirable. Moreover, a strong interface bond results in high shear strength of the composite and an effective load transfer to the fibers under longitudinal tensile load. However, a strong interface bond will significantly decrease the ability of the fiber to debond from matrix during fracture process and lowering the composite toughness. This ability is very beneficial especially in brittle fiber

composites because the debonding process can act as crack arrestor and prevent further propagation of the crack.

This study presents an axisymmetric finite element analysis of a penny-shaped crack in a brittle fiber approaching a fiber-matrix interface. The main goal of this study was to determine the influence of fiber-volume fraction for various fiber-to-matrix elastic moduli ratios on possibility of the interface failure either in shear or in tension. Furthermore, the influence of residual stresses and the fiber orthotropy were also examined. The residual stresses arise from the thermal expansion mismatch between fiber and matrix as the composite is cooled down after processing.

1.2 Literature Review

The fiber-volume fraction is one of the parameters employed in analyzing composites. There have been several models developed to address the failure of the composites as function of this parameter. These models are: fiber cracks in dilute fiber-volume fraction composites by Gupta [3], periodic cracks in higher fiber volume fraction composites by Erdogan and Bakioglu [4], and nonhomogenous interfaces and nondilute fiber-volume fractions by Bechel and Kaw [5].

In addition, a number of criteria have been presented in the past by various authors in order to explore the phenomenon of crack deflection at the fiber-matrix interface. He and Hutchinson [6] examined the tendency of the transverse crack impinging on the interface joining two dissimilar materials to penetrate the interface or to deflect into the interface. The materials on either

side of the interface are elastic and isotropic. They presented criteria that compared the energy release rate for the deflected crack to the maximum energy release rate for a penetrating crack $\frac{\Gamma_d}{\Gamma_p}$. This result can be compared to ratio of the toughness of the interface to the mode I toughness of uncracked material $\frac{\Gamma_{ic}}{\Gamma_c}$. The impinging crack is most likely to be deflected into the interface if

$$\frac{\Gamma_{ic}}{\Gamma_c} < \frac{\Gamma_d}{\Gamma_p} \tag{1}$$

because the condition for propagation into the interface will be met at a lower load than that for penetration across the interface. The crack will tend to penetrate the interface when the inequality is reversed.

Swenson and Rau [7] studied the plain strain problem of a crack terminating perpendicular to the interface between two isotropic half spaces with different elastic constants. They concluded that the probability of an interface failure in shear or in tension is very highly influenced by modulus ratio of the two isotropic half spaces. A crack in the stiffer material will likely cause the interface to fail in shear, whereas the crack in softer material will lead to tensile splitting of the interface.

Cornie et al. [8] came up with the criteria that addressed the fiber-matrix debonding. The debonding can be expressed in terms of cohesive strength of the interface, shear strength of the interface, and fiber fracture stress. They found that if the ratio of the interface cohesive strength (normal or shear) to the

fiber strength is less than the ratio of the normal (or shear) stress at the interface to axial stress at the crack tip the tendency of the crack to deflect along the interface is higher.

Pagano [9] investigated the transverse matrix crack impinging on the fiber-matrix interface in a brittle matrix composite. In this study, he constructed general material design curves for fiber penetration and interface debonding for multiple fiber-to-matrix ratios. These curves allow a comparison between potential energy release rate and a material toughness value to make initial assessment of the success of failure of a composite made from a particular combination of materials.

CHAPTER 2

FINITE ELEMENT MODEL DESIGN

2.1 Geometry and Boundary Conditions

The analysis of a penny-shape crack located in a brittle fiber was performed using the finite element software package ANSYS® 8.0. To simulate a fracture behavior of the cracked fiber and the resulting stresses, a representative volume element (RVE) consisting of a single fiber surrounded by cylindrical tubes of matrix and composite, respectively, was used as illustrated in Figure 2. The RVE is considered to represent the composite and to respond in the same way as the whole composite [10].

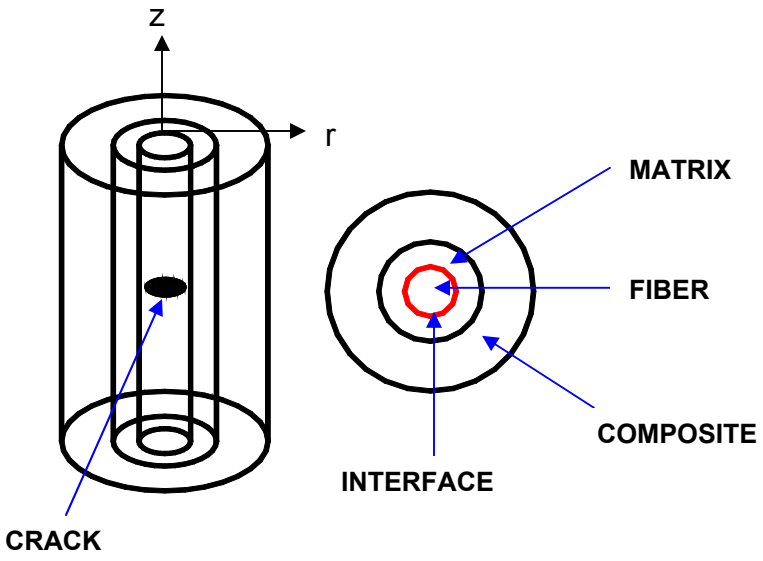

Figure 2: The Representative Volume Element

The finite element model was designed as 2-D axisymmetric structure in the r-z plane. The use of an axisymmetric model greatly reduced the modeling and analysis time compared to that of an equivalent 3-D model. The geometry and boundary conditions of the finite element model are schematically represented in Figure 3. Due to symmetry in the geometry and the boundary conditions the finite element calculations were performed on the right upper quadrant of the representative volume unit shown in Figure 2. The boundary conditions for the finite element model were taken as:

1. at $z = 0$
   a) u_z=0 for $a \le r \le W$
   b) σ_{rz}=0, σ_{zz}=0 for $0 < r < a$
2. at $z = L$
   a) u_z=prescribed uniform displacement, $0 \le r \le W$
   b) σ_{rz}=0, $0 \le r \le W$
3. at $r = 0$
   a) u_r=0 for $0 \le z \le L$
   b) σ_{rz}=0, $0 \le z \le L$
4. at $r = W$
   a) σ_{rz}=0, $0 \le z \le L$
   b) σ_{rr}=0, $0 \le z \le L$

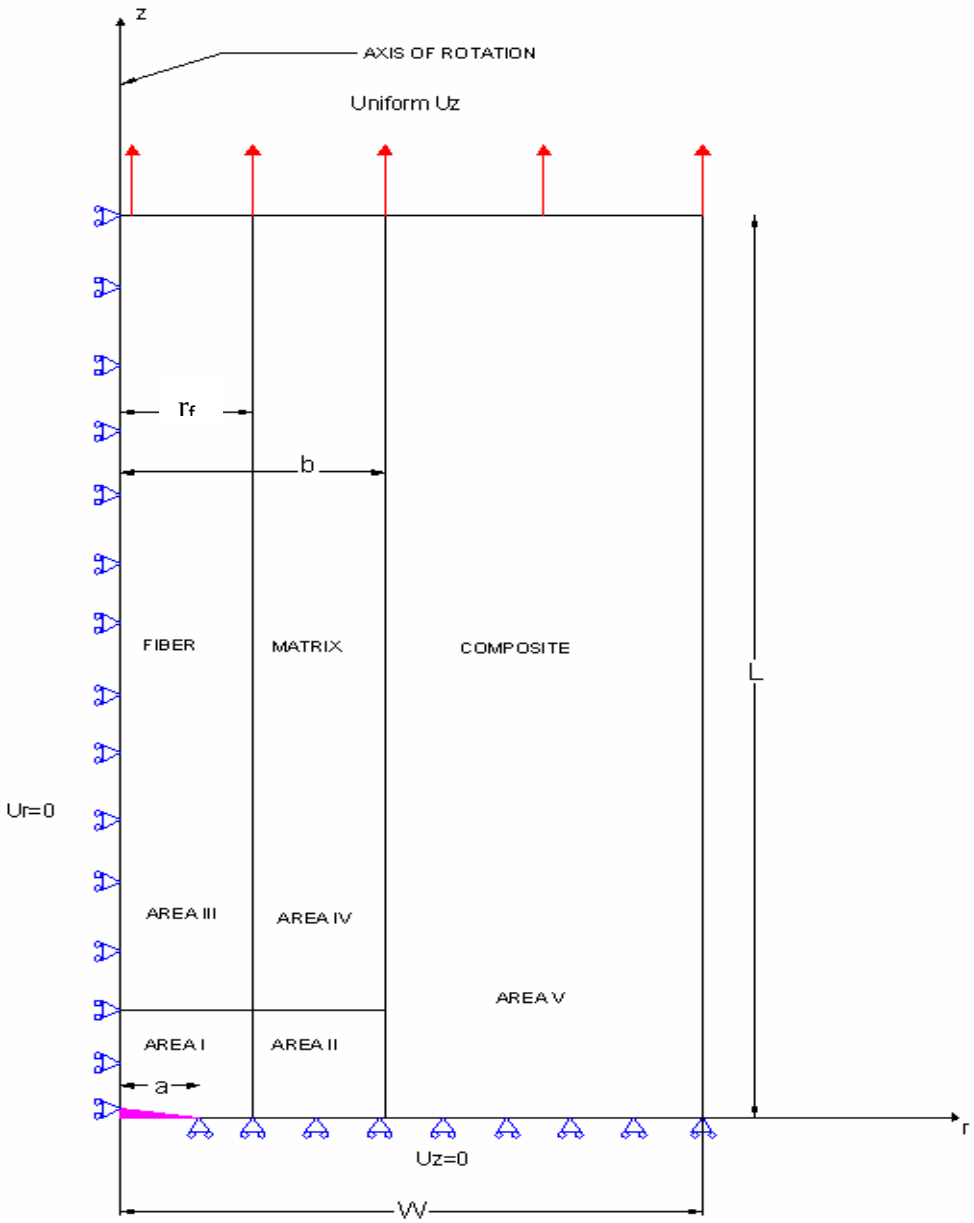

Figure 3: Schematic Representation of Finite Element Model

Also, the mode of deformation is axisymmetric so the non-zero stress and displacement components depend only on r and z and are independent of θ.

The 6-node triangular element (Plane 2) with a quadratic displacement behavior that was used for all the analyses performed in this study is shown in Figure 4. The dimensions of the finite element model were 10 units wide and 30 units high and were kept constant throughout the entire study.

The finite element software used to carry out the finite element computations in this study supported only a limited number of nodes (128,000).

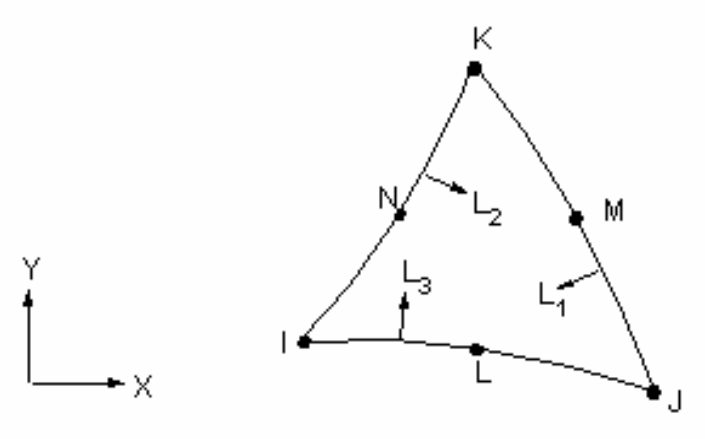

Figure 4: Plane2 Element

Consequently, the model was subdivided into five separate areas to allow greater concentration of elements in the regions in which the stress gradient was expected to be high, such as the crack tip and fiber-matrix interface (Area I and Area II). The remaining areas had significantly lower concentrations of elements. On average, there were 120,000 nodes and 60,000 elements in each model.

The fiber of unit radius (r_f) is comprised of Area I and Area III. Also, the Area I contains crack of radius a. The radius b of the two concentric cylinders representing fiber and matrix was calculated based on the fiber-volume fraction given by

$$V_f = \frac{r_f^{\,2}}{b^2} \tag{2}$$

The three fiber-volume fractions used in the analysis were: 0.25, 0.50, 0.75 and the corresponding b values were: 2, 1.414 and 1.155, respectively.

The fiber containing the penny-shaped crack is parallel to the longitudinal axis (z axis) and the crack plane z=0 is oriented perpendicular to that axis. The fiber-matrix interface was modeled as perfectly bonded. Furthermore, the composite was subjected to uniform and constant longitudinal tensile strain in the positive z direction and therefore was displacement controlled. As a consequence, the crack experiences Mode I loading. Figure 5 shows the shapes of deformed and undeformed finite element model.

The Linear Elastic Fracture Mechanics (LEFM) approach was used as a means to obtain stress field caused by the presence of the crack. This approach was justified due to the brittle nature of the fiber. Because the stresses are singular in the region immediately surrounding the crack tip and vary as $\frac{1}{\sqrt{d}}$, where d is the distance from the crack tip, the triangular quadratic elements were employed with their midside nodes shifted by a quarter toward the crack tip.

The elements were arranged in semicircle around the crack tip, one element every 30 degrees. Figure 6 illustrates the element arrangement in the crack tip vicinity.

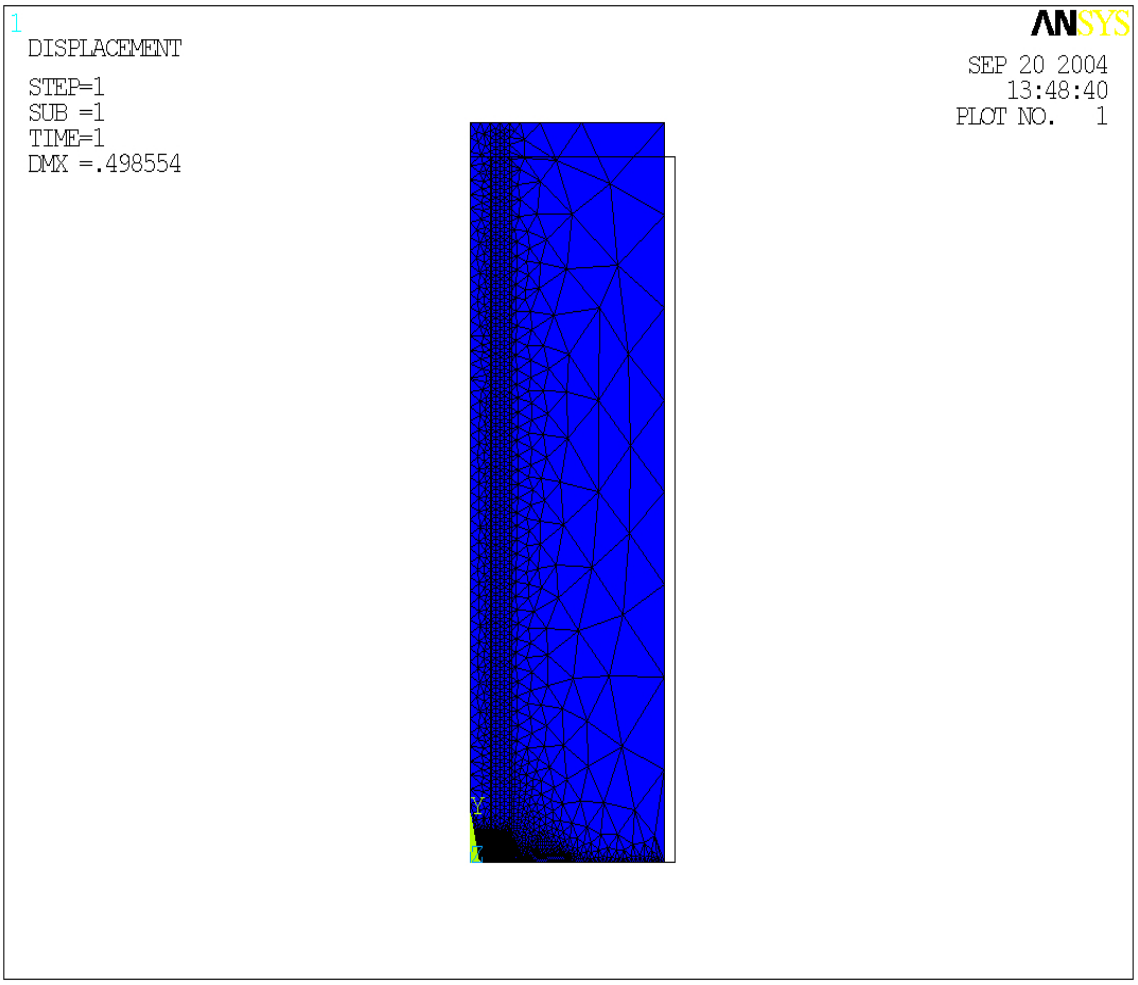

Figure 5: Deformed and Undeformed Shapes of Finite Element Model

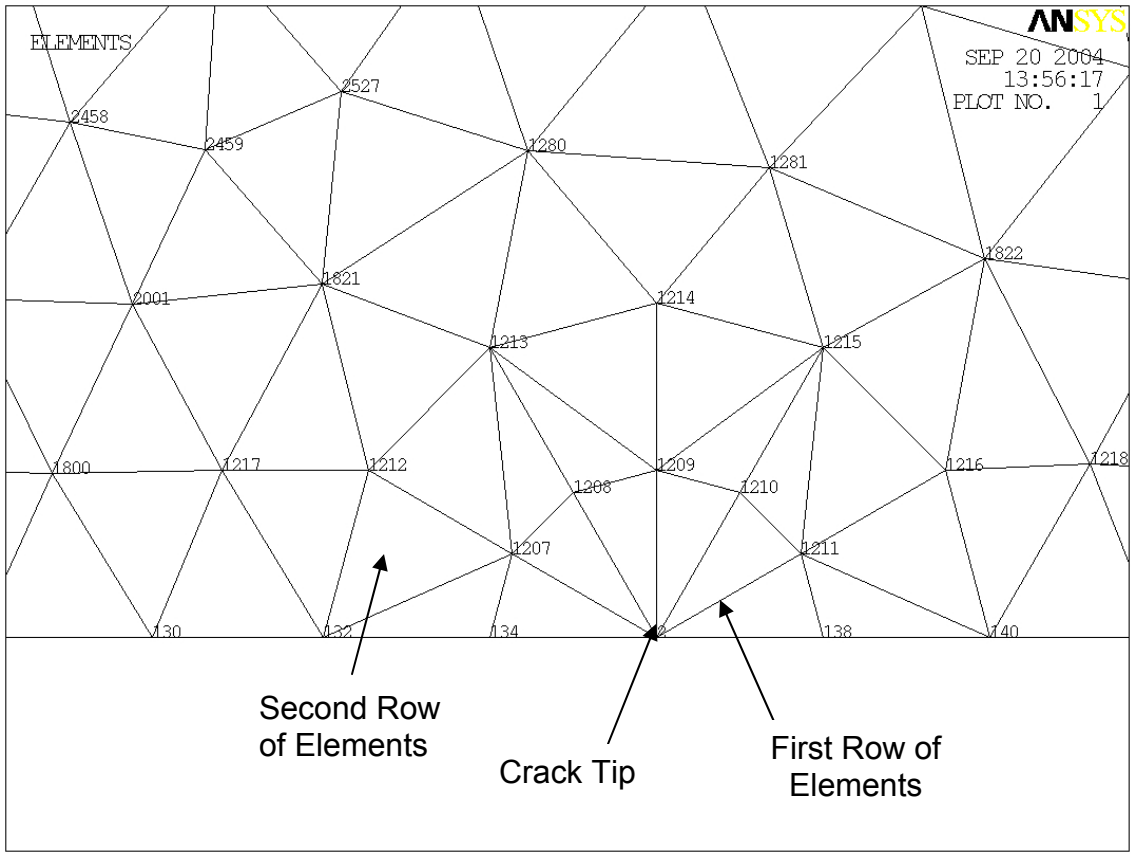

Figure 6: The Crack Tip in the Finite Element Model

2.2 Fundamental Equations

The majority of a unidirectional fiber-reinforced composites are classified either as an orthotropic or transversely isotropic materials. This classification is based on the geometric fiber arrangement in the matrix. A unidirectional fiber-reinforced composite with fibers arranged in hexagonal or random manner in the plane perpendicular to the fibers axes, as shown in Figure 7, is considered to be transversely isotropic.

HEXAGONAL RANDOM

Figure 7: Cross-Sections of Composites with Hexagonal and Random Fiber Arrangement

The transversely isotropic material requires only five engineering constants to fully describe its elastic behavior. The engineering constants are: E_{zz}, E_{rr}, ν_{zr}, G_{zr}, $G_{r\theta}$. By considering fibers to be along z-axis in the cylindrical coordinate system, then the r-θ plane becomes isotropic and there is no preferred direction in that plane. The following subsections list equations [11] that were used to calculate engineering constants needed to describe composite material. The equations are part of Input Files written for finite element software. The sample of an Input File is located in Appendix 1.

2.2.1 Isotropic Fiber, Isotropic Matrix

The following are the equations used for calculating material properties of the composite consisting of isotropic fiber and isotropic matrix.

1.Elastic Moduli

a. Longitudinal $$E_{zz} = V_f \cdot E_f + V_m \cdot E_m + \left[\frac{4V_f V_m (\nu_m - \nu_f)^2}{\left(\frac{V_f}{k_m}\right) + \left(\frac{V_m}{k_f}\right) + \left(\frac{1}{G_m}\right)} \right] \quad (3)$$

where,

V_f is the fiber volume fraction

V_m is the matrix volume fraction

E_f is the elastic modulus of fiber

E_m is the elastic modulus of matrix

G_m is the shear modulus of matrix

ν_f is the Poisson's ratio of fiber

ν_m is the Poisson's ratio of matrix

k_f is the plane-strain bulk modulus of fiber

k_m is the plane-strain bulk modulus of matrix

b. Transverse $$E_{rr} = E_{\theta\theta} = \frac{E_m}{1 - \left[\sqrt{V_f} \left(1 - \frac{E_m}{E_f} \right) \right]} \quad (4)$$

2. Poisson's Ratios

a. $$\nu_{zr} = \nu_{z\theta} = V_f \nu_f + V_m \nu_m + \left\{ \frac{V_f V_m (\nu_f - \nu_m)\left[\left(\frac{1}{k_m}\right) - \left(\frac{1}{k_f}\right)\right]}{\left(\frac{V_f}{k_m}\right) + \left(\frac{V_m}{k_f}\right) + \left(\frac{1}{G_m}\right)} \right\} \quad (5)$$

b. $$\nu_{r\theta} = 1 - E_{rr}\left(\frac{2\nu_{zr}^{\ 2}}{E_{zz}} + \frac{1}{2k}\right) \quad (6)$$

where,

k the is plane-strain bulk modulus

3. Shear Moduli

a. $$G_{zr} = G_{z\theta} = G_m \left[\frac{G_f (1 + V_f) + G_m V_m}{G_f V_m + G_m (1 + V_f)} \right] \quad (7)$$

where,

G_f is the shear modulus of fiber

b. $$G_{r\theta} = \frac{E_{rr}}{2(1 + \nu_{r\theta})} \quad (8)$$

where,

$$G_f = \frac{E_f}{2(1 + \nu_f)} \quad (9)$$

$$G_m = \frac{E_m}{2(1 + \nu_m)} \quad (10)$$

4. Bulk Modulus

$$k_2 = \frac{\left(k_f + G_m\right) + V_f G_m \left(k_f - k_m\right)}{k_f + G_m - V_f \left(k_f - k_m\right)} \tag{11}$$

where,

$$k_f = \frac{E_f}{2\left(1-2\nu_f\right)\left(1+\nu_f\right)} \tag{12}$$

$$k_m = \frac{E_m}{2\left(1-2\nu_m\right)\left(1+\nu_m\right)} \tag{13}$$

2.2.2 Transversely Isotropic Fiber, Isotropic Matrix

The following are the equations used for calculating material properties of the composite consisting of transversely isotropic fiber and isotropic matrix.

1.Elastic Moduli

a. Longitudinal $E_{zz} = E_{f1} V_f + E_m V_m$ (14)

b. Transverse $E_{rr} = E_{\theta\theta} = \dfrac{E_m}{1 - \left[\sqrt{V_f}\left(1 - \dfrac{E_m}{E_{f22}}\right)\right]}$ (15)

2. Shear Moduli

a. $G_{zr} = G_{z\theta} = \dfrac{G_m}{1 - \sqrt{V_f}\left(1 - \dfrac{G_m}{G_{f_{zr}}}\right)}$ (16)

b. $$G_{r\theta} = \frac{G_m}{1-\sqrt{V_f}\left(1-\frac{G_m}{G_{f_{r\theta}}}\right)} \quad (17)$$

3. Poisson's Ratios

a. $$\nu_{zr} = \nu_{z\theta} = \nu_{f_{zr}} V_f + \nu_m V_m \quad (18)$$

b. $$\nu_{r\theta} = \frac{E_{rr}}{2G_{r\theta}} - 1 \quad (19)$$

4. Coefficients of Thermal Expansion

a. Longitudinal $$\alpha_{zz} = \frac{E_{f_{zz}} \alpha_{f_{zz}} V_f + E_m \alpha_m V_m}{E_{f_{zz}} V_f + E_m V_m} \quad (20)$$

b. Transverse $$\alpha_{rr} = V_f \alpha_{f_{rr}} \left(1+\nu_{f_{zr}}\right) + V_m \alpha_m \left(1+\nu_m\right) - \left(V_f \nu_{f_{zr}} + V_m \nu_m\right) \alpha_{zz} \quad (21)$$

where,

α_f is the coefficient of thermal expansion of fiber

α_m is the coefficient of thermal expansion of matrix

CHAPTER 3

FINITE ELEMENT MODEL VALIDATION

Solving the same test problem with analytical and finite element method assessed the accuracy of the finite element model. The values of u_z, u_r, σ_{rr}, σ_{zz}, σ_{rz}, and $\sigma_{\theta\theta}$ obtained from the analysis of the finite element model at chosen locations (r, z) were compared to the values obtained at the same locations by using analytical analysis of the same model. Linear elastic and isotropic material behavior was assumed for the finite element and analytical model (E=30×10^6 and ν=0.3). Moreover, the assumption of perfect fiber-matrix interface was made. The stress field in the analytical method was determined by superposition of two boundary value problems, one hosting a crack, the other being uncracked as illustrated in Figure 8.

In Figure 8a, an uncracked cylinder is subjected to a uniform boundary traction p in the z direction. This created the following stresses: σ_{zz} =p, σ_{rr} =0, $\sigma_{\theta\theta}$ =0, and σ_{rz} =0. Because of the isotropic material assumption, the Hooke's law in cylindrical coordinates was used as a basis for displacements derivation in r and z directions, respectively.

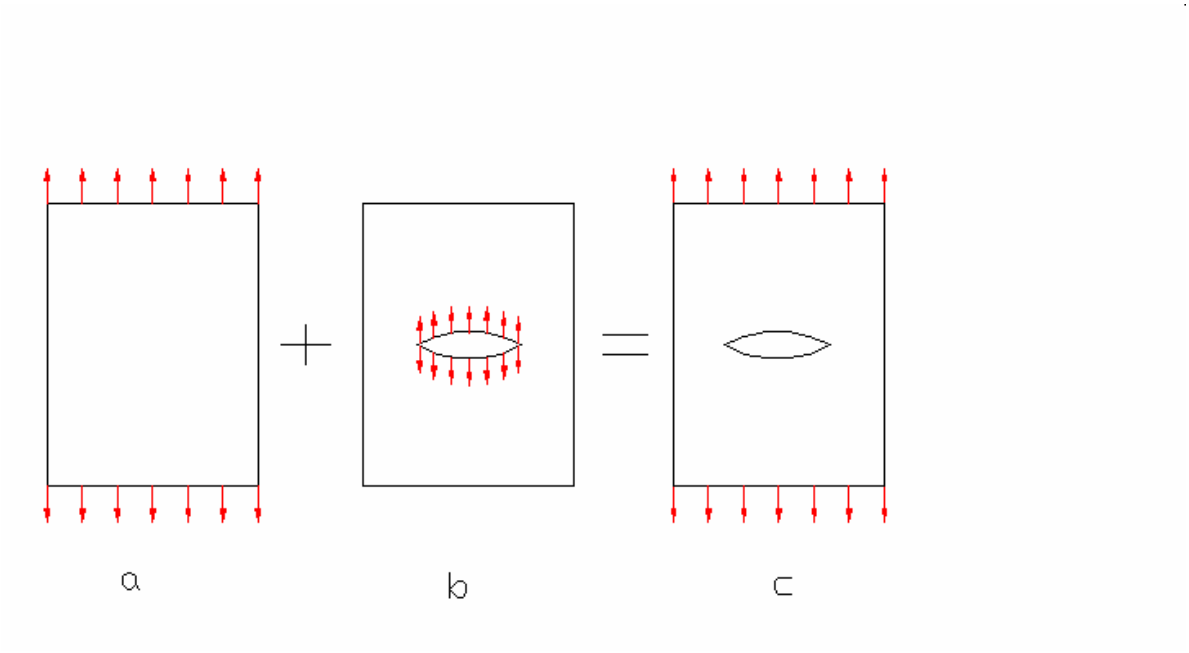

Figure 8: Principle of Superposition

$$\varepsilon_{rr} = \frac{1}{E}\left[\sigma_{rr} - v\left(\sigma_{zz} + \sigma_{\theta\theta}\right)\right] \tag{22}$$

and because

$$\sigma_{zz} = p\,, \quad \sigma_{rr} = 0 \;\,, \; \sigma_{\theta\theta} = 0$$

ε_{rr} simplifies to

$$\varepsilon_{rr} = \frac{-vp}{E} \tag{23}$$

Therefore,

$$u_r = \varepsilon_{rr} r \tag{24}$$

Similarly,

$$u_z = \varepsilon_{zz} z \tag{25}$$

Figure 8b shows traction p applied on the crack face. To obtain the values for u_z, u_z, $\sigma_{rr}, \sigma_{zz}, \sigma_{rz}$, and $\sigma_{\theta\theta}$, a system of differential equations [12] was solved using a code written in Maple® 9.0 (see Appendix 2). Due to the symmetry, the problem can be reduced to the half space $(z > 0, 0 \le r < \infty)$ with the following conditions on the $z = 0$ plane:

$\sigma_{rz}(r,0,0) = 0 \qquad r \ge 0$ (r=cylinder radius)

$\sigma_{zz}(r,0,0) = -p \qquad 0 \le r < a$ (a=half crack length)

$u_z(r,0,0) = 0 \qquad r > a$

A single potential function $f(r,z)$ was employed which automatically frees plane $z = 0$ from shear stress σ_{rz}. The displacement and stress components are then written in terms of that function:

$$u_r = (1-2\nu)\frac{\partial f}{\partial r} + z\frac{\partial^2 f}{\partial r \partial z} \tag{26}$$

$$u_z = -2(1-\nu)\frac{\partial f}{\partial z} + z\frac{\partial^2 f}{\partial z^2} \tag{27}$$

$$\sigma_{rr} = 2\mu\left[(1-2\nu)\frac{\partial^2 f}{\partial r^2} - 2\nu\frac{\partial^2 f}{\partial z^2} + z\frac{\partial^3 f}{\partial r^2 \partial z}\right] \tag{28}$$

where,

μ is the shear modulus of elasticity

ν is the Poisson's ratio

$$\sigma_{\theta\theta} = 2\mu\left[\frac{1}{r}\frac{\partial f}{\partial r} + 2\nu\frac{\partial^2 f}{\partial r^2} + \frac{z}{r}\frac{\partial^2 f}{\partial r \partial z}\right] \tag{29}$$

$$\sigma_{zz} = 2\mu\left[-\frac{\partial^{2} f}{\partial z^{2}} + z\frac{\partial^3 f}{\partial z^3}\right] \tag{30}$$

$$\sigma_{rz} = 2\mu z\frac{\partial^3 f}{\partial r \partial z^2} \tag{31}$$

By using Fourier-Hankel transform, the function $f(r,z)$ of two variables is expressed in terms of the function $A(s)$, which depends only on the variable s. The function $A(s)$ is found by solving the following dual integral:

$$A(s) = \frac{-1}{\pi\mu}\int_0^a \sin(st)dt\int_0^t \frac{rp(r)dr}{\left(t^2 - r^2\right)^{\frac{1}{2}}} \tag{32}$$

where,

p is the normal traction

The solution of the above equation is inserted into the equation for $f(r,z)$.

$$f(r,z) = \int_0^\infty \frac{A(s)}{s} J_0(rs)e^{(-sz)ds} \tag{33}$$

where,

$f(r,z)$ is the potential function of two variables

J_0 is the Bessel function of order zero

This, in turn, enables us to find the two displacements and four stress components. The final values of the analytical analysis are obtained by adding results from part a and b as shown in Figure 8c. This was done using Mathcad®8.0 (Appendix 3).

The finite element model was constructed as described in chapter 2. In order to achieve desired accuracy of results, the convergence of a finite element solution was conducted. The purpose of the convergence study was to refine the mesh size so that the relative error between analytical and finite element solutions was less than one percent.

Table 1 lists the percentages of relative errors at different locations along the interface and in the matrix of the composite. The highest error was 0.1 percent.

Table 1: Percentage Error Values of Five Nodal Locations

Nodal Coordinates	u_r	u_z	σ_{rr}	$\sigma_{\theta\theta}$	σ_{zz}	σ_{rz}
r=1.00000 z=0.02379	0.0126	0.0102	0.033	0.031	0.093	0.031
r=1.00000 z=0.05293	0.0128	0.0101	0.057	0.01	0.088	0.055
r=1.01329 z=0.03118	0.0127	0.1	0.026	0.017	0.093	0.057
r=1.03737 z=0.02182	0.0129	0.096	0.025	0.015	0.089	0.072
r=1.03107 z=0.05283	0.0129	0.1	0.019	0.032	0.086	0.074

CHAPTER 4

FINITE ELEMENT MODEL ANALYSIS

The finite element model analysis was divided into several separate parts. Each part of the analysis investigated the influence of a single criterion on the possibility of the interface failure. The following are the criteria used in the analysis:

1. Fiber-Volume Fraction (FVF)
2. Fiber Orthotropy
3. Thermal Stress

For each criterion, the normalized length of the fiber crack, $\frac{a}{r_f}$, was progressively increased from 0.6 to 0.97. Furthermore, each criterion was analyzed at 0.25, 0.50, and 0.75 fiber-volume fractions.

4.1 Fiber-Volume Fraction Criterion

The first part of the FVF analysis focused on how the fiber-volume fraction affects the interface tensile and shear failure for different fiber-to-matrix elastic moduli ratios. There were four moduli ratios used in the analysis as follows:

1. $\frac{E_f}{E_m}$ =1 represents composite with fiber and matrix made of the same material
2. $\frac{E_f}{E_m}$ =6 represents typical ceramic matrix composite
3. $\frac{E_f}{E_m}$ =20 represents typical polymer matrix composite such as glass/epoxy
4. $\frac{E_f}{E_m}$ =80 represents typical polymer matrix composite such as graphite/epoxy

Each moduli ratio was analyzed at 0.25, 0.50 and 0.75 fiber-volume fractions. The fiber and matrix were assumed to be linear elastic and isotropic with the same Poisson's ratios. Table 2 lists fiber and matrix properties used in the analysis.

Table 2: Material Properties of Constituents in the Fiber-to-Matrix Moduli Ratio Analysis

PROPERTY	SYMBOL	FIBER	MATRIX
Modulus of Elasticity	E	1, 6, 20, 80	1
Poisson's Ratio	ν	0.3	0.3

The displacement u_z was taken as 0.1, which constitutes 10% of the fiber radius.

The second part of the FVF analysis involved examining the influence of fiber-volume fraction and two different longitudinal displacements on interface failure in silicon carbide/epoxy composite. The two displacements used in the

above analysis were calculated based on the fiber ultimate tensile strength. The first displacement was obtained by calculating displacement value needed to create tensile stress in the fiber equal to the ultimate tensile strength of that fiber, henceforth called 100% displacement. The second displacement was taken as a half of the first one, henceforth called 50% displacement. Table 3 lists the properties of fiber and matrix for silicon carbide/epoxy composite [13,14]. Table 4 contains displacements and interface strengths used in performing the analysis of silicon carbide/epoxy composite [15].

Table 3: Material Properties of Fiber and Matrix in Silicon Carbide/Epoxy Composite

PROPERTY	SYMBOL	FIBER	MATRIX
Elastic Modulus	E	400 [GPa]	3.44 [GPa]
Poisson's Ratio	ν	0.15	0.35
Fiber Ultimate Tensile Strength	σ_{fib}	3450 [MPa]	
Matrix Ultimate Tensile Strength	σ_{mat}		69.29 [MPa]
Coefficient of Thermal Expansion	α	0	60 [$\mu m/m/^{\circ}C$]

Table 4: Displacements and Interface Strengths Used in Silicone Carbide/Epoxy Analysis

100 % Displacement applied	u_z	0.25875	0.25875
50 % Displacement applied	u_z	0.12938	0.12938
Interface Normal Strength	σ_{int}	35 [MPa]	
Interface Shear Strength	τ_{int}	32.5 [MPa]	

4.2 Orthotropic Fiber Criterion

To determine the influence of the orthotropic fiber on the interface failure, two graphite/epoxy composites were used for analysis with the fiber and matrix properties listed in Tables 5 and 6 [16]. For comparison purposes, isotropic and orthotropic fibers were used. The analysis was performed for 0.25, 0.50, and 0.75 fiber-volume fractions. The applied displacement u_z was calculated based on ultimate tensile strength of the graphite fiber. The applied displacement, u_z, in both cases was 0.46587.

Table 5: Material Properties of Orthotropic Fiber and Isotropic Matrix in Graphite/Epoxy

PROPERTY	SYMBOL	FIBER	MATRIX
Longitudinal Elastic Modulus	E_{zz}	260 [GPa]	3.5 [GPa]
Transverse Elastic Modulus	$E_{rr}, E_{\theta\theta}$	14 [GPa]	3.5 [GPa]
Shear Modulus	$G_{zr}, G_{z\theta}$	50.95 [GPa]	
Shear Modulus	$G_{r\theta}$	8.27 [GPa]	
Poisson's Ratio	$\nu_{zr}, \nu_{z\theta}$	0.26	0.35
Poisson's Ratio	$\nu_{r\theta}$	0.33	0.35
Ultimate Tensile Strength	σ_{fib}	4038 [MPa]	

Table 6: Material Properties of Isotropic Fiber and Matrix in Graphite/Epoxy Composite

PROPERTY	SYMBOL	FIBER	MATRIX
Elastic Modulus	E	260 [GPa]	3.5 [GPa]
Poisson's Ratio	v	0.26	0.35
Ultimate Tensile Strength	σ_{fib}	4038 [MPa]	

4.3 Thermal Stress Criterion

The thermal stresses are created as a result of a mismatch in thermal expansion coefficients of fiber and matrix. The graphite/epoxy composite having different fiber and matrix thermal expansion coefficients was analyzed. The obtained results were then compared to the results for the same composite analyzed without thermal expansion coefficients. Each composite was analyzed at 0.25, 0.50, and 0.75 fiber-volume fractions. The displacement u_z was calculated based on ultimate tensile strength of a graphite fiber. Table 7 lists material properties for fiber and matrix in the thermal stress analysis of graphite/epoxy composite. The applied displacement, u_z, was 0.46857

Table 7: Material Properties of Graphite/Epoxy Used for Thermal Stress Analysis

PROPERTY	SYMBOL	FIBER	MATRIX
Longitudinal Elastic Modulus	E_{zz}	260 [GPa]	3.5 [GPa]
Transverse Elastic Modulus	$E_{rr}, E_{\theta\theta}$	14 [GPa]	3.5 [GPa]
Shear Modulus	$G_{zr}, G_{z\theta}$	50.95 [GPa]	
Shear Modulus	$G_{r\theta}$	8.27 [GPa]	
Poisson's Ratio	$\nu_{zr}, \nu_{z\theta}$	0.26	0.35
Poisson's Ratio	$\nu_{r\theta}$	0.33	0.35
Coefficient of Thermal Expansion	α_{zz}	-0.855 [$\mu m/m/^{\circ}C$]	90[$\mu m/m/^{\circ}C$]
Coefficient of Thermal Expansion	$\alpha_{rr}, \alpha_{\theta\theta}$	3.24 [$\mu m/m/^{\circ}C$]	90[$\mu m/m/^{\circ}C$]
Ultimate Tensile Strength	σ_{fib}	4038 [MPa]	

In order to determine how each criterion plays a role in influencing the possibility of shear and tensile interface failure, the following stress ratios were calculated: $\frac{\sigma_{rr(\max)}}{\sigma_1}$ and $\frac{\sigma_{rz(\max)}}{\sigma_1}$ for each crack length. Those ratios were then plotted as a function of normalized crack length, $\frac{a}{r_f}$, for the three fiber-volume fractions. The preceding ratios provide us with the qualitative means to determine and to compare the influence of different parameters on the two types of the interface failures. This comparison is not only possible between different fiber-volume fractions of the same composite, but also between composites with various elastic moduli ratios. The $\sigma_{rr(\max)}$, and $\sigma_{rz(\max)}$ stresses represent the maximum tensile and shear stresses along fiber-matrix interface. In turn, the σ_1 represents the largest principal stress present in the matrix. The choice of using principal stress σ_1 instead of $\sigma_{zz(\max)}$ in the above ratios was made based on the fact that principal stress σ_1 was increasing at a higher rate than $\sigma_{zz(\max)}$ as the crack was approaching fiber-matrix interface. To illustrate the difference in values between σ_1 and $(\sigma_{zz})_{\max}$ with increasing crack length, the stress ratios, $\frac{\sigma_1}{(\sigma_{zz})_{\max}}$ were calculated for 0.50 and 0.75 fiber-volume fractions and plotted as a function of normalized crack length. Figure 9 clearly shows that the stress ratios, $\frac{\sigma_1}{(\sigma_{zz})_{\max}}$, for both fiber-volume fractions are higher than one when the crack is close to the fiber-matrix interface.

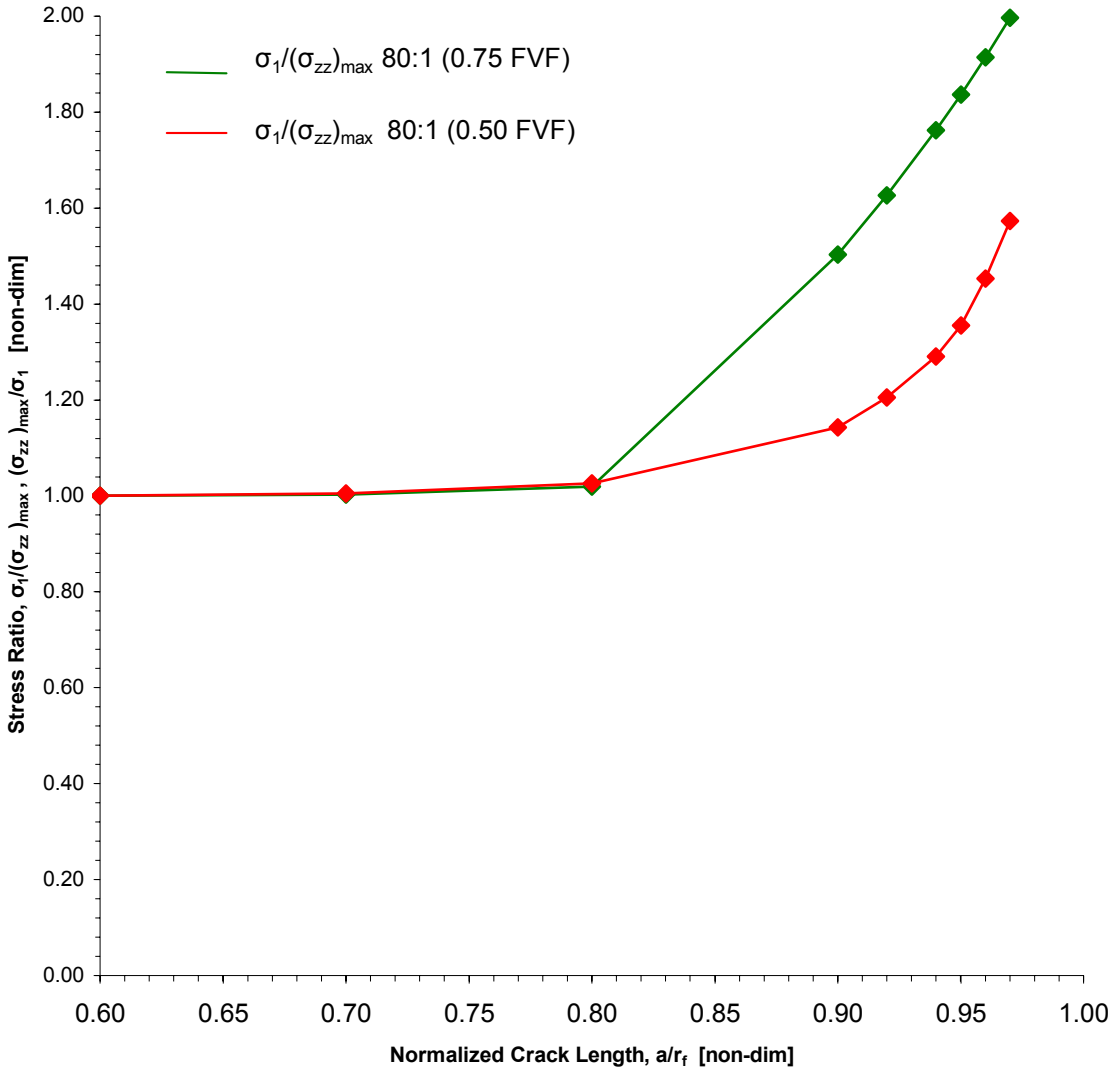

Figure 9: Stress Ratios of $\frac{\sigma_1}{(\sigma_{zz})_{\max}}$ in the Matrix as Function of Normalized Crack Length, $\frac{a}{r_f}$

CHAPTER 5

RESULTS AND DISCUSSION

As mentioned in the previous chapters, in this study, we want to assess how the fiber-volume fraction, fiber orthotropy, and thermal stresses influence the crack propagation path of a cracked fiber – does the crack propagate across the interface to the matrix, or does the crack propagate along the interface. We understand that debonding of fiber-matrix interface causes the blunting of the crack tip, acts as a crack arrestor, and hence contributes to the overall increase in composite toughness. This can be easily accomplished by making a weak fiber-interface, but such weak interfaces decrease transverse compressive and shear strength. Hence, to be able to quantify to build a fiber-matrix interface that is just weak enough to allow interface debonding requires us to fully understand the mechanisms of crack propagation.

The stress ratios used to understand propagation paths of a fiber crack were described in chapter 4 and are used to define the conditions necessary for debonding of fiber-matrix interface in the fiber reinforced composite subjected to longitudinal tensile strain. The debonding at the interface will occur if:

1. The ratio of the maximum tensile stress at the interface, $(\sigma_{rr})_{\max}$, to the largest principal stress in the matrix, σ_1 is greater than the ratio of the interface normal strength, σ_{int}, to the ultimate matrix strength, σ_{mat}, that is,

$$\frac{(\sigma_{rr})_{\max}}{\sigma_1} > \frac{\sigma_{\text{int}}}{\sigma_{mat}} \tag{34}$$

2. The ratio of the maximum shear stress at the interface, $(\sigma_{rz})_{\max}$, to the largest principal stress [8], σ_1, is greater than the ratio of the interface shear strength, τ_{int}, to the ultimate matrix strength, σ_{mat}, that is,

$$\frac{(\sigma_{rz})_{\max}}{\sigma_1} > \frac{\tau_{\text{int}}}{\sigma_{mat}} \tag{35}$$

For a specific composite, the two strength ratios $\frac{\sigma_{\text{int}}}{\sigma_{mat}}$, and $\frac{\tau_{\text{int}}}{\sigma_{mat}}$ are material properties of a particular fiber and matrix combination. These strength ratios are not dependent on fiber-volume fraction. In contrast, the two stress ratios $\frac{(\sigma_{rr})_{\max}}{\sigma_1}$ and $\frac{(\sigma_{rz})_{\max}}{\sigma_1}$ on the left side of the inequalities (Equations 34 and 35) are influenced by several variables such as: crack length, fiber-volume fraction, fiber-to-matrix elastic moduli ratio, fiber orthotropy, and thermal stresses.

The presentation and discussion of the results is divided into three separate parts to study the influence of fiber-volume fraction, fiber orthotropy and thermal stress.

5.1 Fiber-Volume Fraction

5.1.1 Elastic Moduli Ratio $\frac{E_f}{E_m} = 1$

When a composite is made of fiber and matrix that have identical elastic moduli, all fiber-volume fractions represent the same geometry of a fiber surrounded by a matrix of infinite radius. So the normalized stress ratios, $\frac{(\sigma_{rr})_{\max}}{\sigma_1}$ and $\frac{(\sigma_{rz})_{\max}}{\sigma_1}$ as a function of normalized crack length, $\frac{a}{r_f}$ are the same for all fiber-volume fractions as given in Figures 10 and 11. Note the single number given for the normalized crack length of unity.

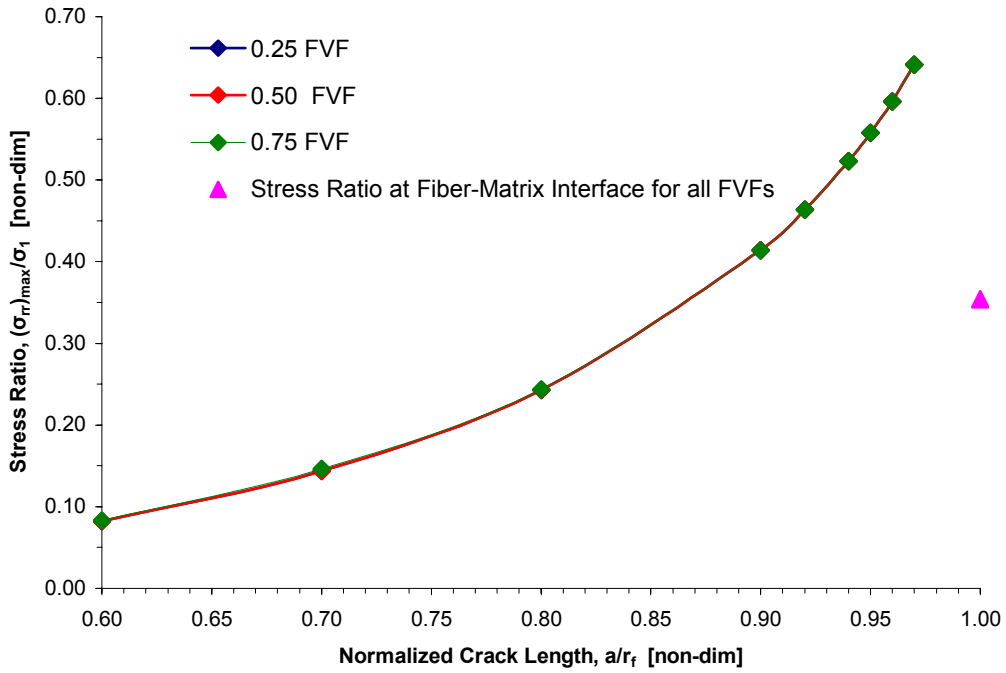

Figure 10: The Stress Ratio, $\frac{(\sigma_{rr})_{\max}}{\sigma_1}$ as a Function of Normalized Crack Length, $\frac{a}{r_f}$ for Elastic Moduli Ratio of $\frac{E_f}{E_m} = 1$

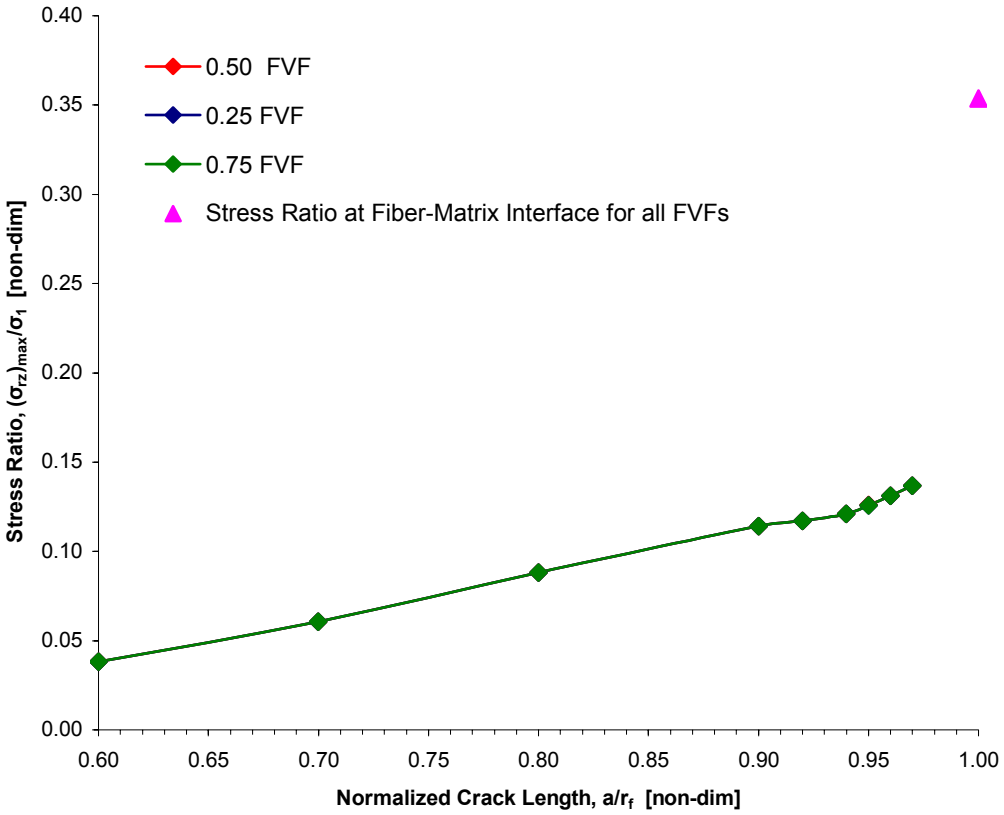

Figure 11: Stress Ratio, $\frac{(\sigma_{rz})_{\max}}{\sigma_1}$ as a Function of Normalized Crack Length, $\frac{a}{r_f}$ for Elastic Moduli Ratio of $\frac{E_f}{E_m} = 1$

5.1.2 Elastic Moduli Ratio $\frac{E_f}{E_m} = 6$

Now let us examine how the fiber-volume fraction affects the crack propagation path for composites where the fiber and matrix elastic moduli are not the same. Figures 12 shows the normalized stress ratio, $\frac{(\sigma_{rr})_{\max}}{\sigma_1}$ as a function of normalized crack length. The trends for fiber-volume fractions of up to 0.5 are

the same, and only for large fiber-volume fractions, the normalized stress, $\frac{(\sigma_{rr})_{\max}}{\sigma_1}$ shows markedly higher values.

Figure 13 show the normalized stress ratios, $\frac{(\sigma_{rz})_{\max}}{\sigma_1}$, as a function of normalized crack length. The trends for all fiber-volume fractions look the same.

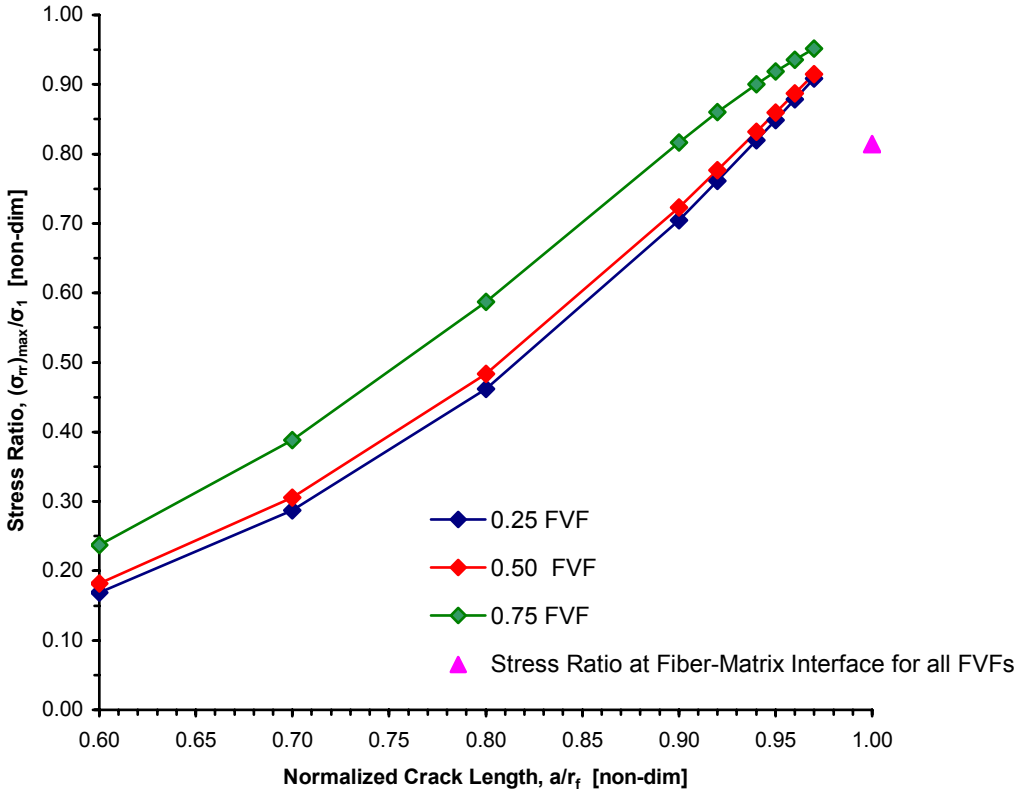

Figure 12: The Stress Ratio, $\frac{(\sigma_{rr})_{\max}}{\sigma_1}$ as a Function of Normalized Crack Length, $\frac{a}{r_f}$ for Elastic Moduli Ratio of $\frac{E_f}{E_m} = 6$

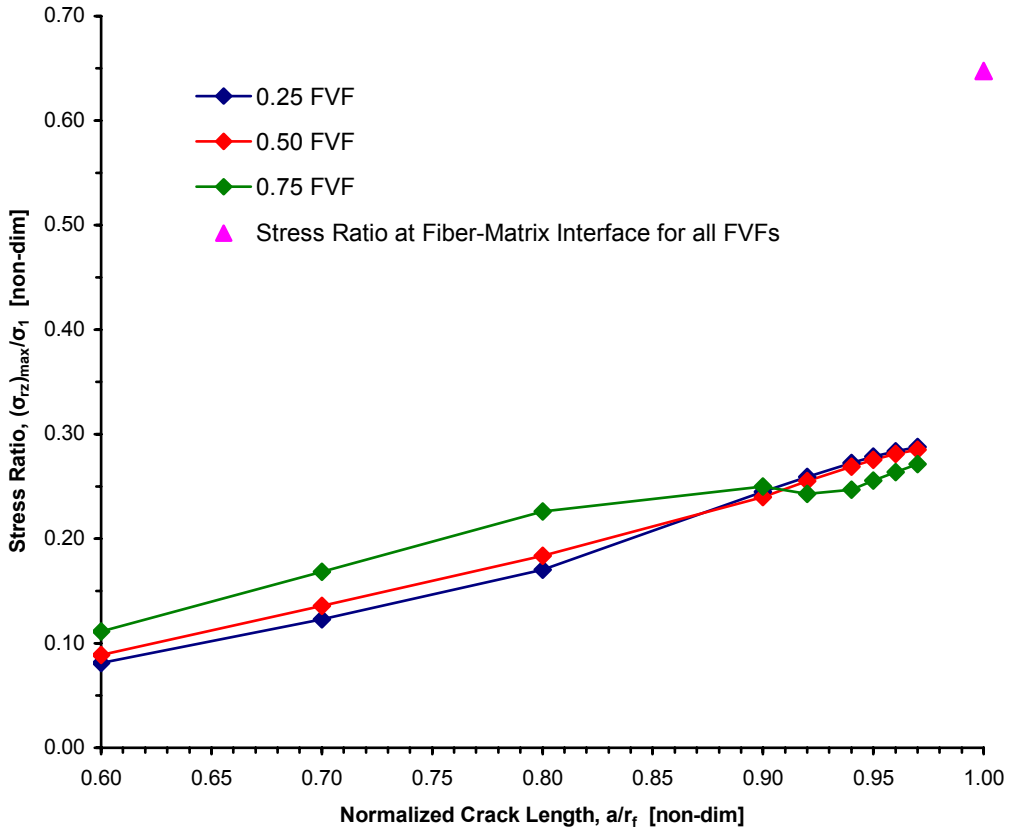

Figure 13: Stress Ratio, $\frac{(\sigma_{rz})_{\max}}{\sigma_1}$ as a Function of Normalized Crack Length, $\frac{a}{r_f}$ for Elastic Moduli Ratio of $\frac{E_f}{E_m} = 6$

5.1.3 Elastic Moduli Ratio $\frac{E_f}{E_m} = 20$

Higher fiber-to-matrix moduli ratios, like $\frac{E_f}{E_m} = 20$ representing a typical glass/epoxy give results in a similar behavior as the case of $\frac{E_f}{E_m} = 6$ except the differences between stress ratio values are more pronounced. This is illustrated in Figures 14 and 15.

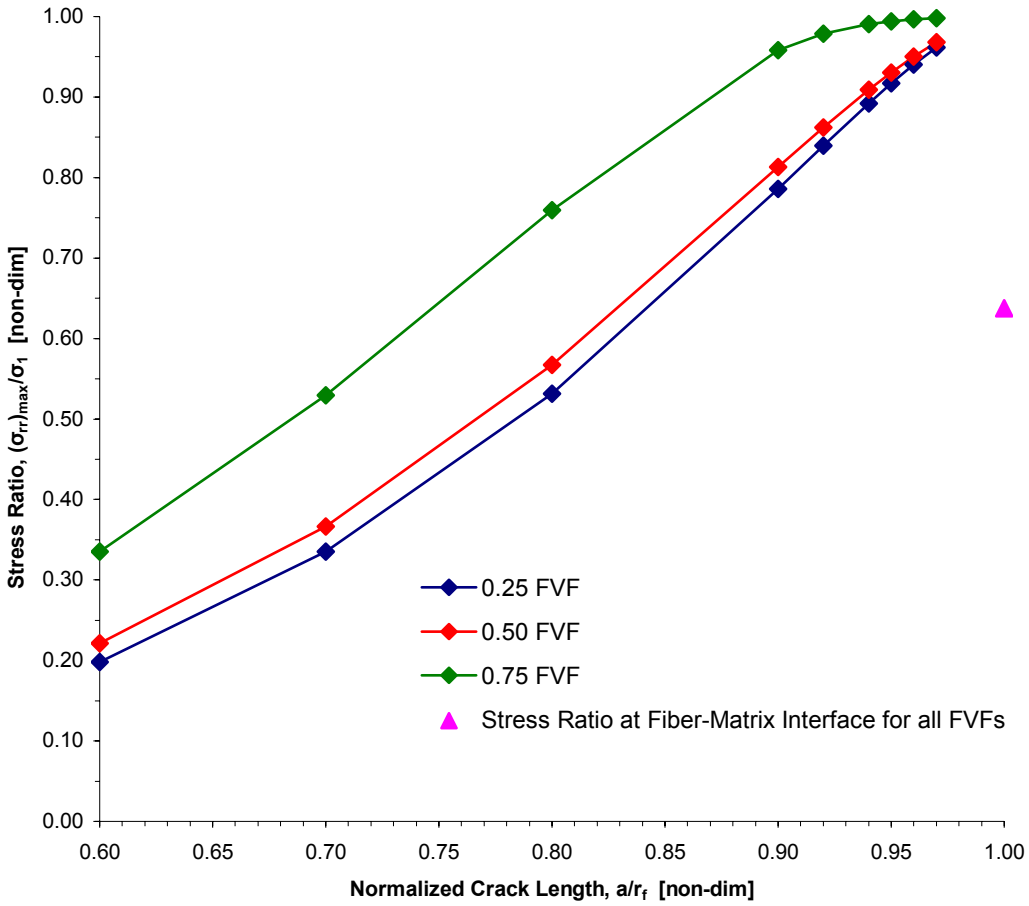

Figure 14: The Stress Ratio, $\frac{(\sigma_{rr})_{\max}}{\sigma_1}$ as a Function of Normalized Crack Length, $\frac{a}{r_f}$ for Elastic Moduli Ratio of $\frac{E_f}{E_m} = 20$

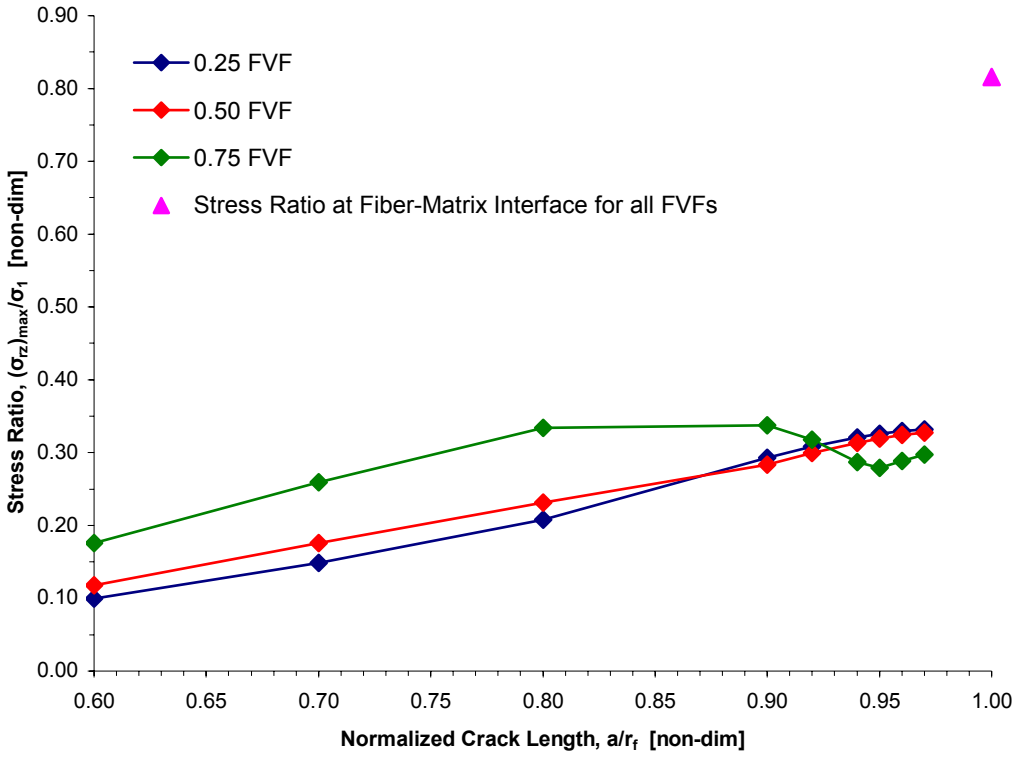

Figure 15: Stress Ratio, $\frac{(\sigma_{rz})_{\max}}{\sigma_1}$ as a Function of Normalized Crack Length, $\frac{a}{r_f}$ for Elastic Moduli Ratio of $\frac{E_f}{E_m} = 20$

5.1.4 Elastic Moduli Ratio $\frac{E_f}{E_m} = 80$

Higher fiber-to-matrix moduli ratios, like $\frac{E_f}{E_m} = 80$ representing a typical graphite/epoxy composite, give results in a similar behavior as the cases of

$\frac{E_f}{E_m} = 6$ and $\frac{E_f}{E_m} = 20$ except the differences between stress ratio values are more pronounced. This is illustrated in Figures 16 and 17.

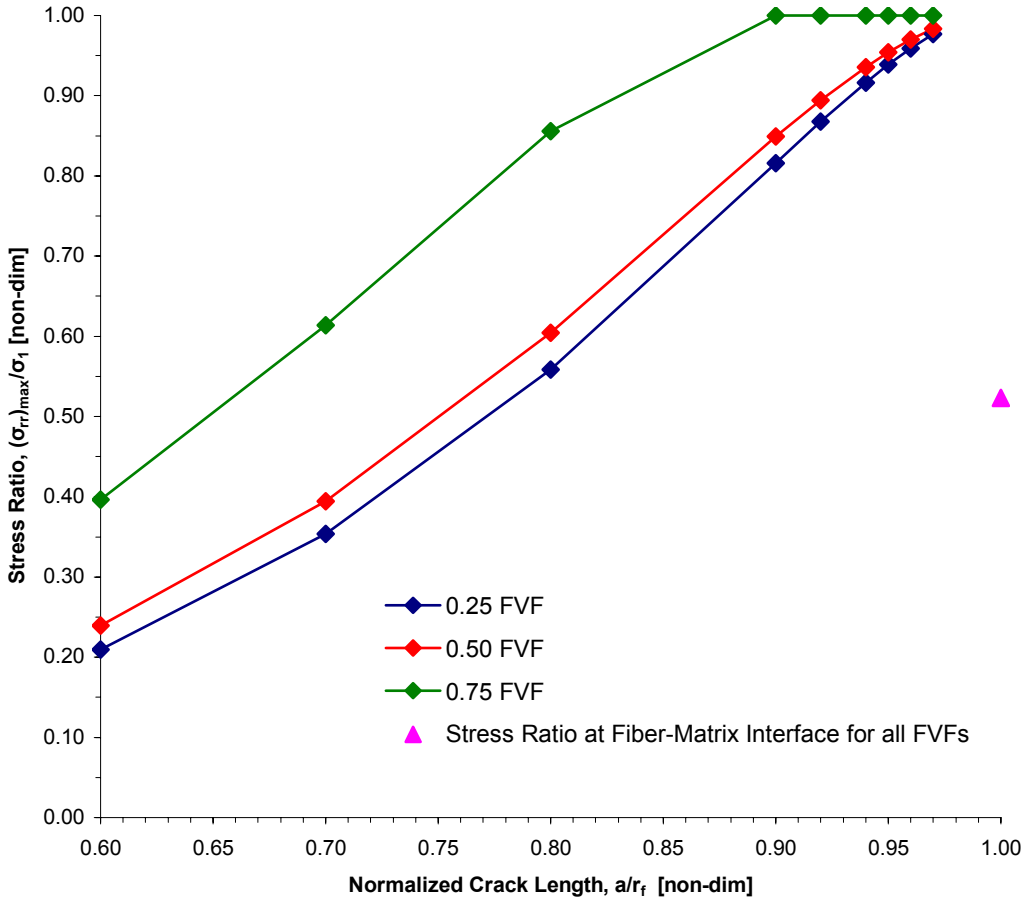

Figure 16: The Stress Ratio, $\frac{(\sigma_{rr})_{\max}}{\sigma_1}$ as a Function of Normalized Crack Length, $\frac{a}{r_f}$ for Elastic Moduli Ratio of $\frac{E_f}{E_m} = 80$

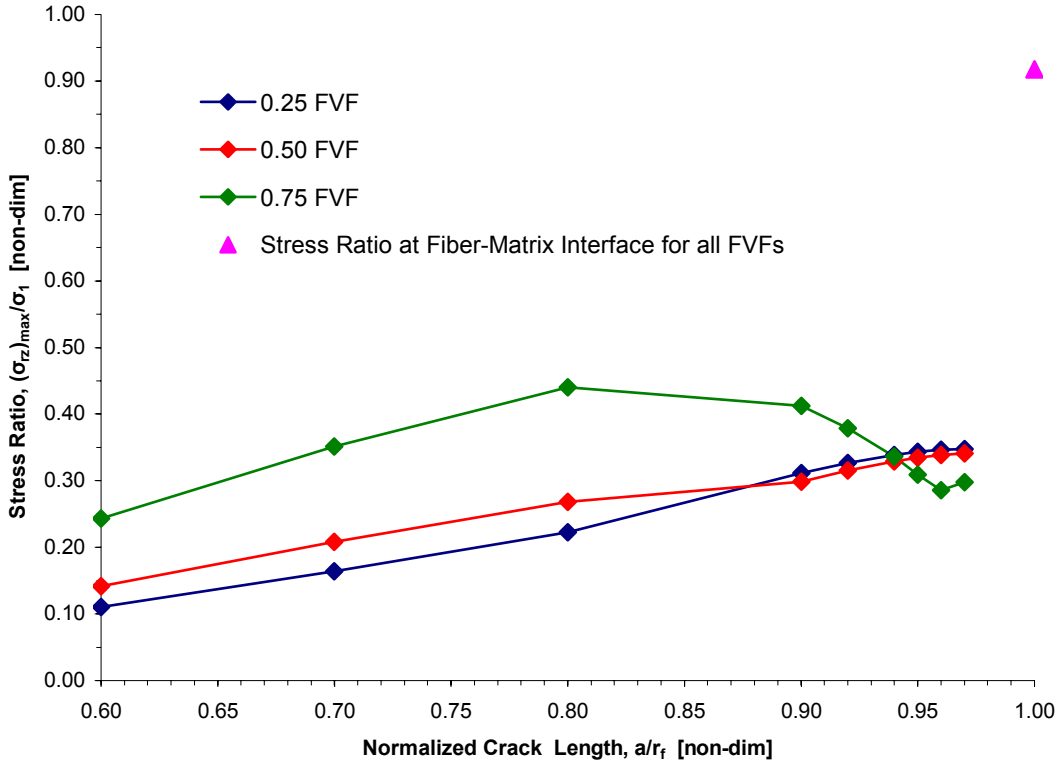

Figure 17: Stress Ratio, $\frac{(\sigma_{rz})_{\max}}{\sigma_1}$ as a Function of Normalized Crack Length, $\frac{a}{r_f}$ for Elastic Moduli Ratio of $\frac{E_f}{E_m} = 80$

The preceding results clearly indicate a substantial influence of fiber-volume fraction on the crack propagation path. The effect is zero for fiber-to-matrix moduli ratio, $\frac{E_f}{E_m} = 1$ and becomes more pronounced as the fiber-to-matrix moduli ratio increases. For large fiber-volume fractions, we see that the possibility of crack propagating along the interface increases, as was observed in experimental studies [1]. This is contrary to recent studies [6,7,8] where crack propagation paths are considered to be independent of fiber-volume fractions.

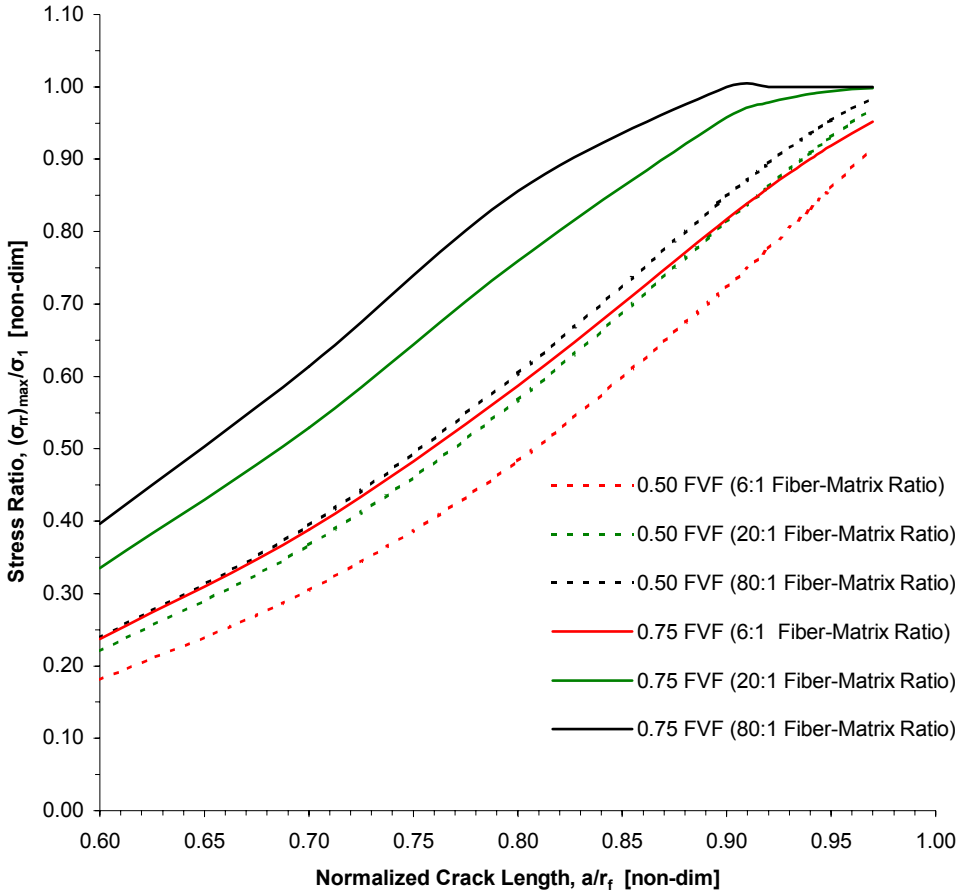

Figure 18: The Influence of Fiber-Matrix-Moduli Ratio and Fiber-Volume Fraction on Tensile Stress Ratio $\frac{(\sigma_{rr})_{\max}}{\sigma_1}$

While the effect of fiber-volume fraction on tensile interface failure was rather straightforward, the same cannot be said about the effect of fiber-volume fraction on interfacial shear failure.

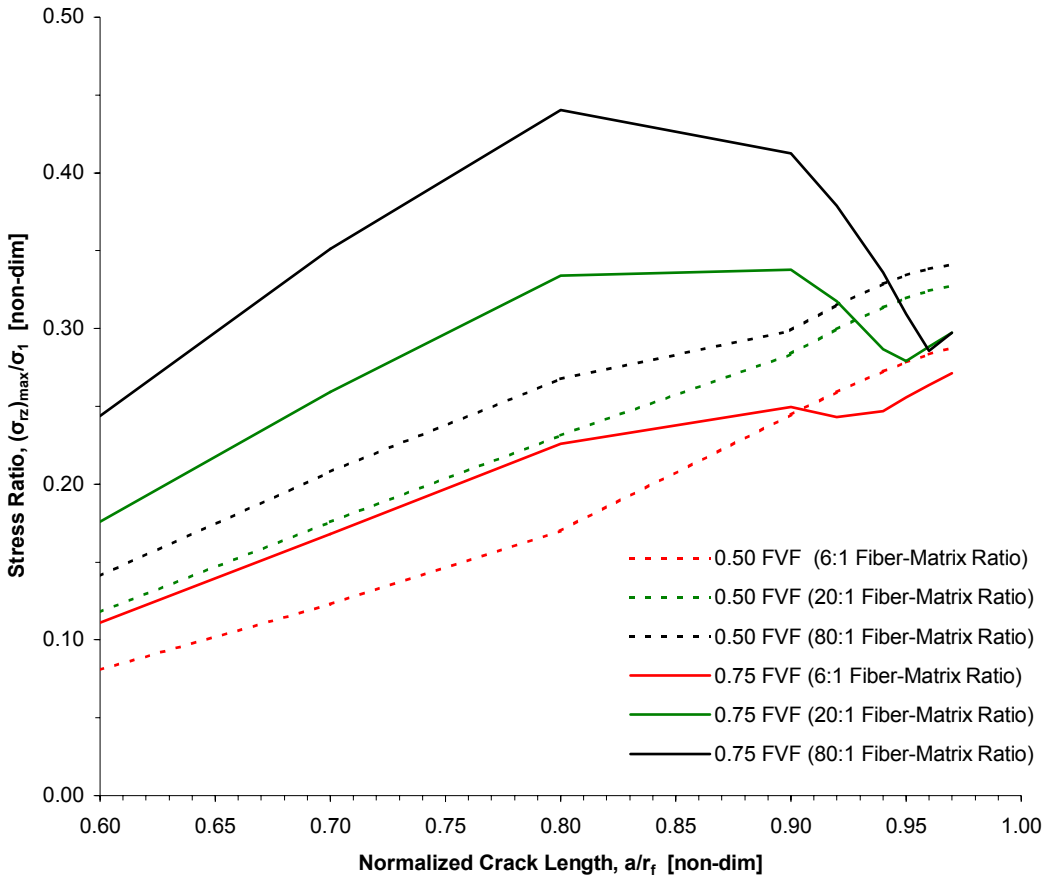

Figure 19: The Influence of Fiber-Matrix Modulus Ratio and Fiber-Volume Fraction on the Shear Stress Ratio $\frac{(\sigma_{rz})_{\max}}{\sigma_1}$

5.1.5 Silicon Carbide/Epoxy Composite

The purpose of analyzing a particular composite system is that we wanted to determine crack propagation path under different remote loading values. We apply strain equal to and then half of the ultimate longitudinal strain of the fiber. The corresponding longitudinal displacements were derived in chapter 4, and are called 100% and 50% displacements, respectively.

Also, we know the ultimate shear and normal strength of the interface for this particular composite system (Table 4). Hence we cannot only find whether the interface fails but also whether it fails due to shear or normal stress in the interface.

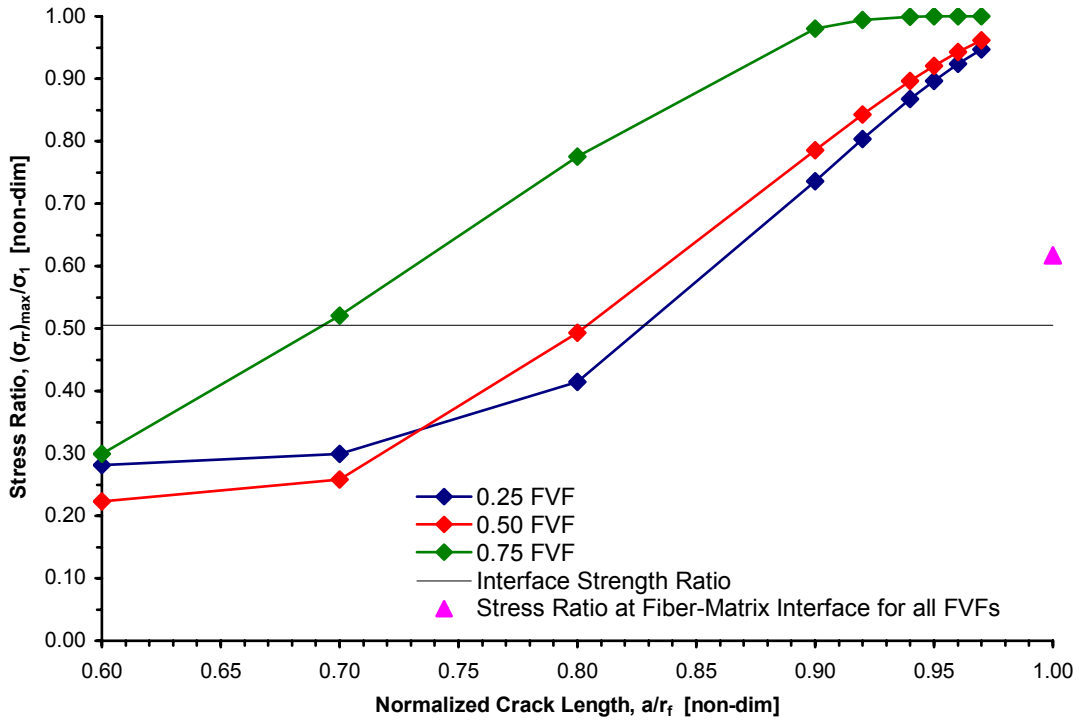

Figure 20: Stress Ratio, $\frac{(\sigma_{rr})_{max}}{\sigma_1}$ as a Function of Normalized Crack Length, $\frac{a}{r_f}$ for Silicon Carbide/Epoxy at 100% Displacement

The Figures 20 and 21 illustrate the behavior of a composite that was subjected to a displacement that created stress in the fiber equivalent to ultimate strength of that fiber. As it can be seen, the interface tensile failure would take place at normalized crack lengths of 0.7 for 0.75 fiber-volume fraction and of 0.8 for 0.25 and 0.50 fiber-volume fractions. Because the $\frac{(\sigma_{rz})_{max}}{\sigma_1}$ stress ratio values

for all three fiber-volume fractions are below the interface strength ratio value throughout the entire crack propagation process, the interface shear failure would not take place.

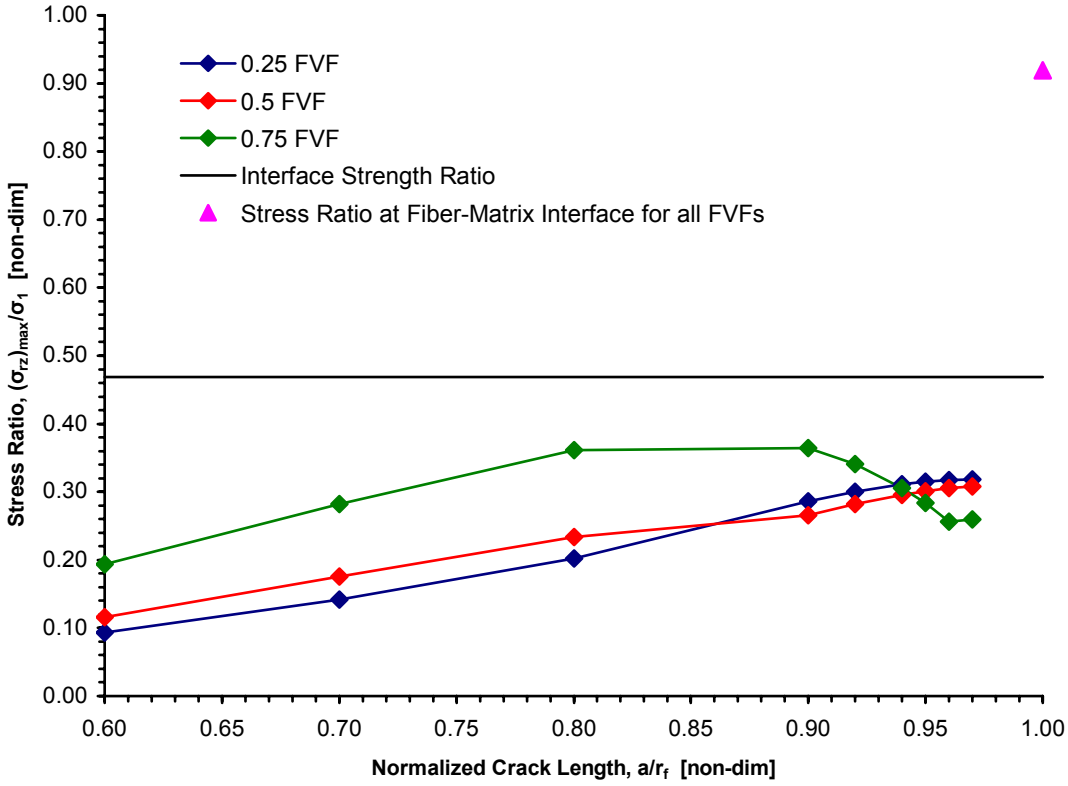

Figure 21: Stress Ratio, $\frac{(\sigma_{rz})_{\max}}{\sigma_1}$ as a Function of Normalized Crack Length, $\frac{a}{r_f}$ for Silicon Carbide/Epoxy at 100% Displacement

To examine the impact of different longitudinal displacements on stress ratios and interface failure mode, the results of two displacements (100% and 50%) were plotted on the same graph, Figures 22 and 23. The graphs clearly show that the reduction in longitudinal displacement by 50% did not affect the stress ratio distribution and interface failure in a significant way.

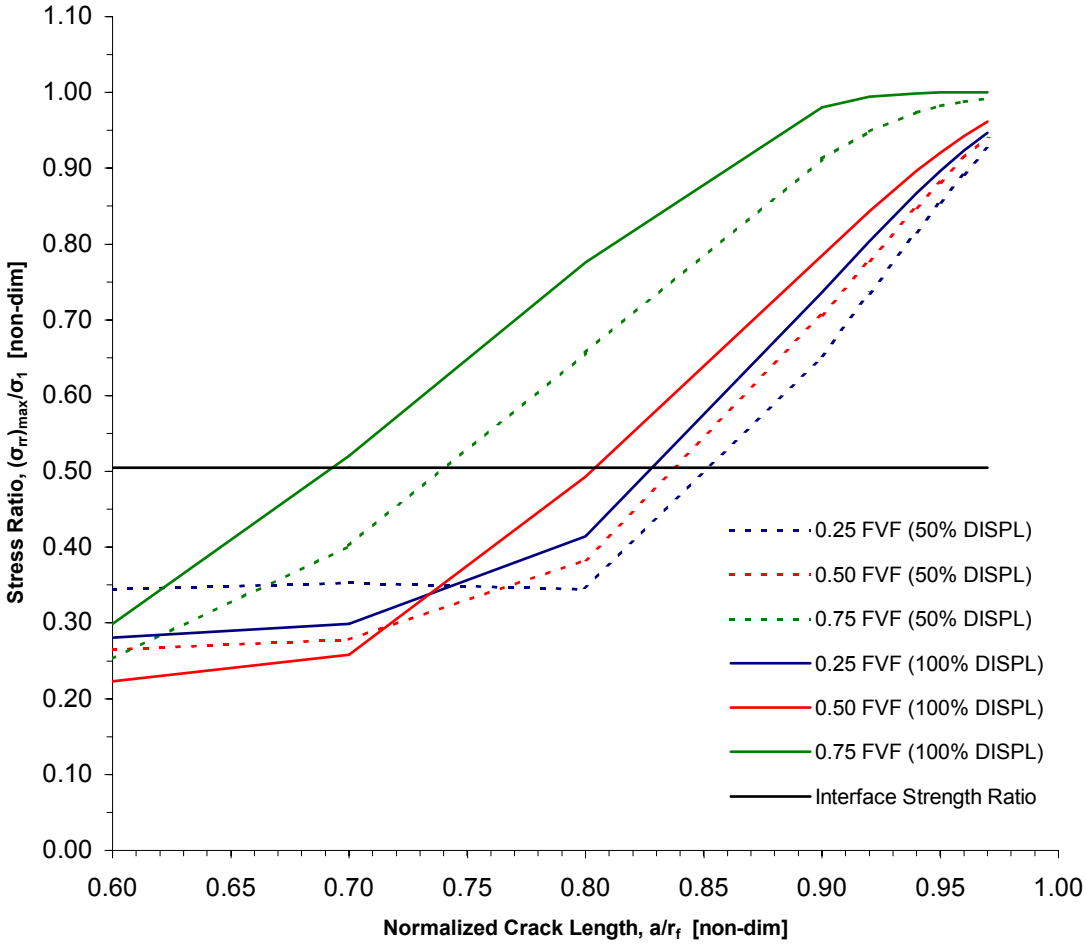

Figure 22: Stress Ratio, $\frac{(\sigma_{rr})_{\max}}{\sigma_1}$ as a Function of Normalized Crack Length, $\frac{a}{r_f}$ for Silicon Carbide/Epoxy at 100% and 50% Displacements

The interface tensile failure for 0.75 fiber-volume fraction would initiate at 0.75 crack length and 0.25 and 0.50 fiber-volume fractions at 0.85 crack length. The interface shear failure as before would not take place because the shear strength ratio is significantly larger than stress ratios present at the fiber-matrix interface.

After running several additional analyses with other smaller displacements, it was found that the shear strength ratio was always higher than the corresponding shear stress ratios. Moreover, the displacements in a 4% to 100% range show that the crack propagation would be along the interface and would be caused by interface tensile failure.

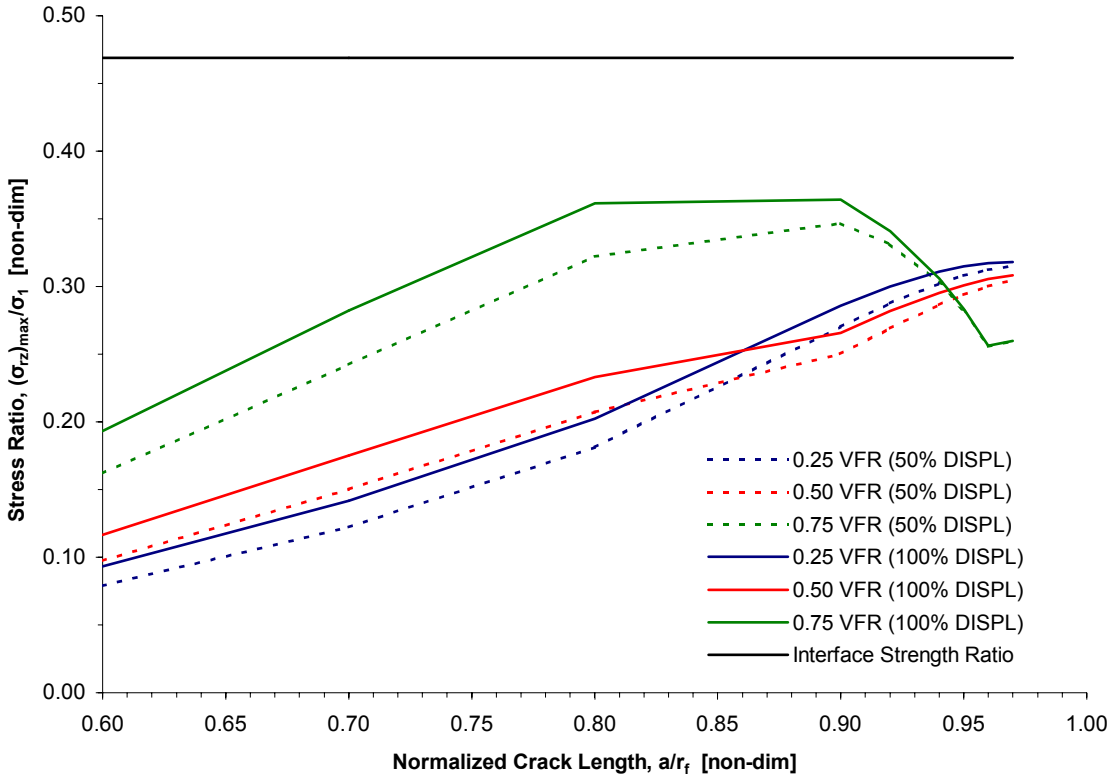

Figure 23: Stress Ratio, $\frac{(\sigma_{rz})_{\max}}{\sigma_1}$ as a Function of Normalized Crack Length, $\frac{a}{r_f}$ for Silicon Carbide/Epoxy at 100% and 50% Displacements

5.2 Fiber Orthotropy

Up to this point, the composites used in this study were assumed to be fibers with isotropic material properties. This section examines what impact fiber

orthotropy have on interface failure. This is accomplished by comparing analysis results of the composite with the orthotropic fiber (transversely isotropic) to the analysis results of the composite with isotropic fiber. In both cases, graphite/epoxy composite is used.

As can be seen in Figure 24, the fiber orthotropic material properties have a unique impact on tensile interface failure. The possibility of interface failure in tension increases with increasing fiber-volume fraction between 0.6-0.9 normalized crack lengths. During this crack growth, the composite with the highest (0.75) fiber-volume fraction is most likely to experience tensile interface failure.

However, when the normalized crack reaches 0.9, the possibility of interface failure in tension for a composite with orthotropic fiber becomes completely independent of fiber-volume fraction. That is, all three fiber-volume fractions generate the same tensile stress ratios. Also, at that point in crack growth, the composite with isotropic fiber and 0.75 fiber-volume fraction has the same chance of experiencing interface tensile failure as the composite with orthotropic fiber.

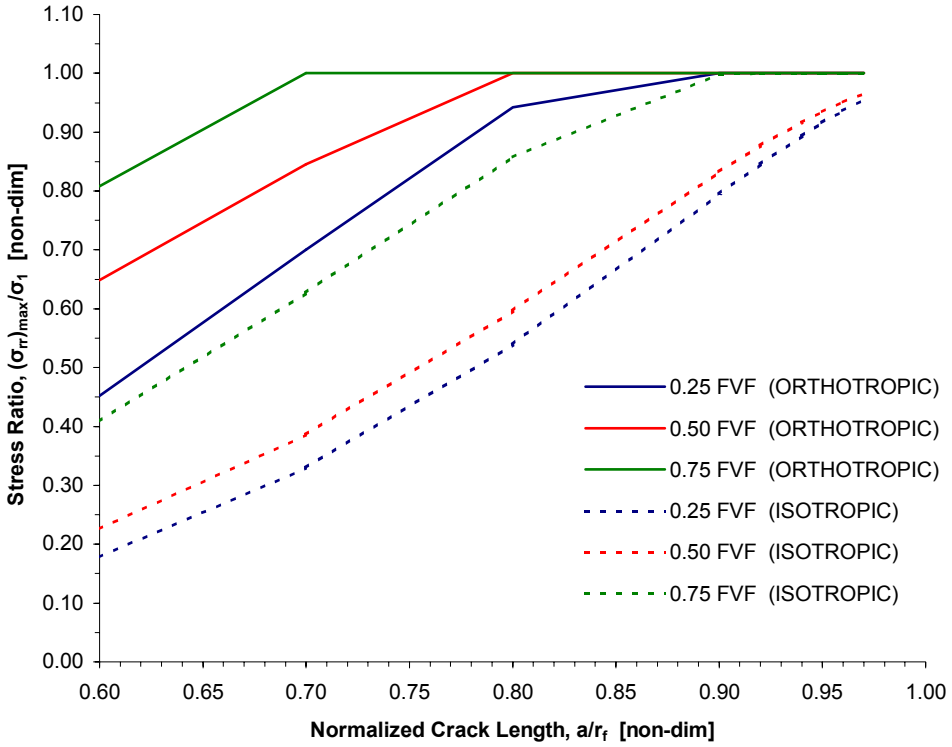

Figure 24: Stress Ratio, $\frac{(\sigma_{rr})_{max}}{\sigma_1}$ as a Function of Normalized Crack Length, $\frac{a}{r_f}$ for Graphite/Epoxy Composite with Orthotropic and Isotropic Fibers

Figure 25 illustrates the effect of orthotropic fiber on interface failure in shear. It can be clearly seen that the presence of orthotropic fiber diminishes the possibility of interface shear failure. As the crack propagates and approaches fiber-matrix interface, the shear stress ratio get progressively smaller. In fact, when the normalized crack length reaches 0.97, the composite with 0.25 fiber-volume fraction has the largest possibility to experience an interface failure in shear.

Also, during the final stage of crack growth, the composites with isotropic fibers are more prone to undergo an interface failure in shear than those with orthotropic fibers.

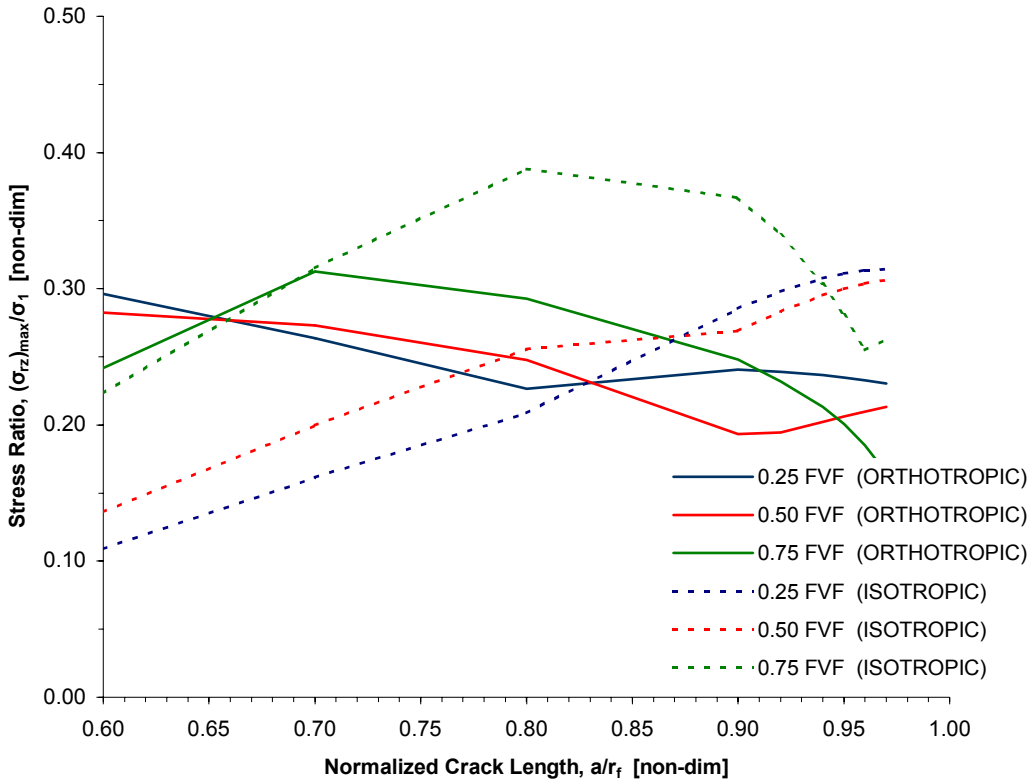

Figure 25: Stress Ratio, $\frac{(\sigma_{rz})_{\max}}{\sigma_1}$ as a Function of Normalized Crack Length, $\frac{a}{r_f}$ for Graphite/Epoxy Composite with Orthotropic and Isotropic Fibers

5.3 Thermal Stress

The thermal stresses in the composite arise due to a mismatch between thermal expansion coefficients of a fiber and a matrix. This mismatch puts the

fiber-matrix interface either in tension or in compression depending which constituent has larger coefficient of thermal expansion.

The thermal strain and the corresponding thermal stress were calculated based on the following equation:

$$\varepsilon_T = \alpha(\Delta T) \tag{36}$$

where,

ε_T is the thermal strain

α is the coefficient of thermal expansion, and

ΔT is the difference between the ambient and processing temperatures,

$$\Delta T = (T - T_{REF})$$

The processing was taken to be T_{REF} =170º C and the final temperature was assumed to be a room temperature at T = 20º C. The resulting negative ΔT indicates shrinkage of both components during the cooling process.

To examine the influence of thermal stress on interface failure, two identical composites, one in presence and other in absence of thermal stresses, were analyzed and the results were compared. The composite used in the analysis was graphite/epoxy with material properties listed in section 4.3.

By looking at Figure 26, it can be concluded that thermal stresses reduce the possibility of interface failure in tension. Because the analyzed composite had $\alpha_m > \alpha_f$, the resulting compressive stress normal to the interface makes debonding from crack in fiber less likely.

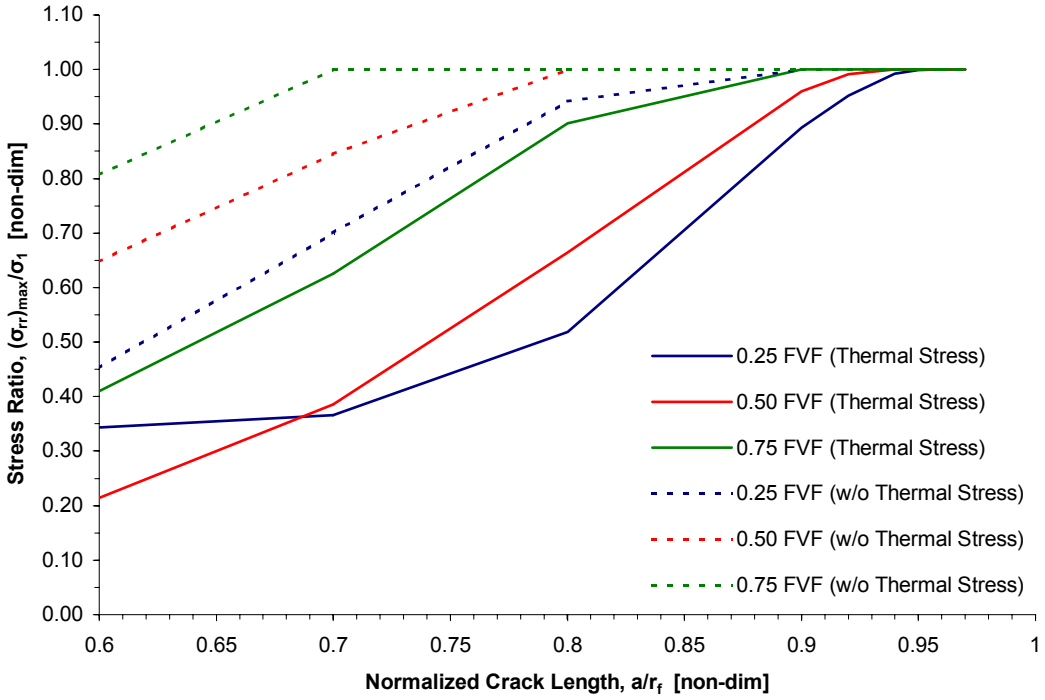

Figure 26: Stress Ratio, $\frac{(\sigma_{rr})_{\max}}{\sigma_1}$ as a Function of Normalized Crack Length, $\frac{a}{r_f}$ for Graphite/Epoxy Composite With and Without Thermal Load Present

The Figure 27 illustrates the impact of thermal stress on interface failure in shear. For the composite with thermal stress present, the shear stress ratios are significantly lower during crack propagation between normalized crack lengths of 0.6 to 0.8 but for larger cracks, the differences between the shear stress ratios among the same fiber-volume fractions are almost negligible.

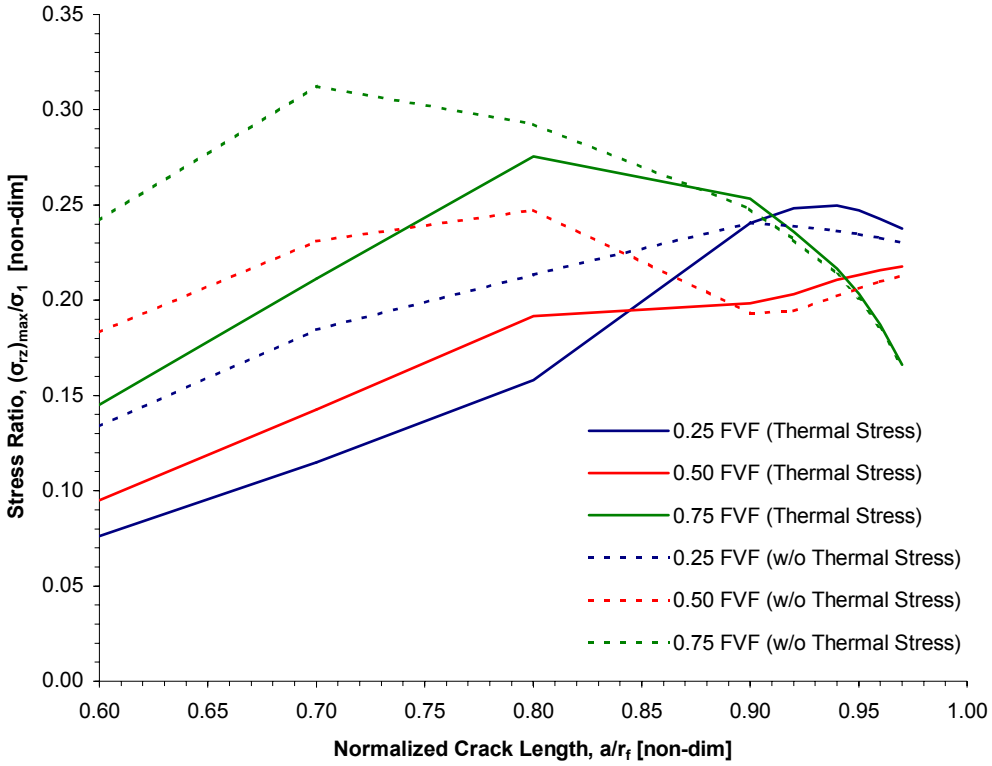

Figure 27: Stress Ratio, $\frac{(\sigma_{rz})_{\max}}{\sigma_1}$ as a Function of Normalized Crack Length, $\frac{a}{r_f}$ for Graphite/Epoxy Composite With and Without Thermal Load Present

CHAPTER 6

CONCLUSIONS

The conclusions gathered from the results of this study can be summarized as follows:

1. The fiber-volume fraction has a profound influence on interface failure
   a) The possibility of interface tensile failure increases with higher fiber-volume fraction
   b) The interface tensile failure is more likely to occur for composites with high fiber-volume fraction and high fiber-to-matrix moduli ratio
   c) The increase of fiber-volume fraction from medium to high makes the interface shear failure more likely during initial crack growth but the possibility diminishes as the crack approaches the fiber-to-matrix interface.
2. The interface in the silicon carbide/epoxy will never fail in shear regardless of the fiber-volume fraction and displacement applied.
3. The tensile interface failure in the silicon carbide/epoxy will take place between 4% and 100% of ultimate longitudinal strain.
4. In the early and middle stages of crack growth, the presence of orthotropic fiber in the graphite/epoxy composite increases the likelihood of tensile interface failure with increasing fiber-volume fraction. During the final stage

of crack propagation the tensile interface failure is not influenced by fiber-volume fraction.

5. The fiber orthotropy in the graphite/epoxy composite diminishes the likelihood of interface failure in shear.
6. The presence of thermal stress in the graphite/epoxy composite lowers the possibility of interface failure in tension and in shear.

REFERENCES

1. Agarwal B.D., Broutman L.J*., Analysis and Performance of Fiber Composites*, John Wiley and Sons, New York, 1980, pp. 46-48

2. Chawla K.K., *Ceramic Matrix Composites*, Chapman and Hall,1993, pp. 300-304

3. Gupta G.D., A Layered Composite with a Broken Laminate, International *Journal of Solids and Structures*, 1973, 9, pp. 1141-1154

4. Erdogan F. and Bakioglu M., Fracture of Plates which Consist of Periodic Dissimilar Strips*, International Journal of Fracture Mechanics*, 1976, 12, pp. 71-84

5. Bechel V.T., Kaw A.K., Fracture Mechanics of Composites with Nonhomogenous Interfaces and Nondilute Fiber Volume Fractions, *International Journal of Solids and Structures*, 1994, 31(15), pp. 2053-2070

6. He M., Hutchinson J. W., Crack Deflection at an Interface Between Dissimilar Elastic Materials, *International Journal of Solids and Structures*, 1989, 25(9), pp. 1053-1067

7. Swenson D. O., Rau Jr. C. A., The Stress Distribution Around a Crack Perpendicular to an Interface Between Materials*, International Journal of Fracture Mechanics*, 1970, 6(4), pp. 357-365

8. Cornie J. A., Argon A. S., Designing Interfaces in Inorganic Matrix Composites*, MRS Bulletin*, 1991, 16(4), pp. 32-38

9. Pagano N. J., *On the Micromechanical Failure Modes in a Class of Ideal Brittle Matrix Composites. Part 2. Uncoated-Fiber Composites*, Composites Part B, 1998, 29B, pp. 121-130

10. Kaw A.K., *Mechanics of Composite Materials*, CRC Press, 1997, pp. 180-181

11. Chawla K.K., *Ceramic Matrix Composites*, Chapman and Hall, 1993, pp. 207-210

12. Kassir M. K., Sih G. C., *Mechanics of Fracture Volume 2: Three-Dimensional Crack Problems*, Noordoff International Publishing, 1975, pp. 2-5

13. *Properties of SCS Fibers*, http://www.specmaterials.com/silicarbsite.htm (Accessed 10/11/2004)

14. *Online Material Data Sheet*, http://www.matweb.com (Accessed 10/11/2004)

15. Tandon G.P., Kim Y. R., *Construction of the Fiber-Matrix Interfacial Failure Envelope in a Polymer Matrix Composite*, International Journal for Multiscale Computational Engineering, 2004, 2(1), pp. 65-77

16. Base Properties of Graphite Fibers, http://casl.ucsd.edu/data_analysis (Accessed 08/22/2004)

APPENDICES

Appendix 1: Ansys Input File

```
/PREP7
ET,1,PLANE2, , ,1
A=0.9


K,1,0,0
K,2,A,0
K,3,1,0
K,4,1.155,0
K,5,10,0
K,6,10,30
K,7,1.155,30
K,8,1,30
K,9,0,30
K,10,0,1.2
K,11,1,1.2
K,12,1.155,1.2

! LINES

L,1,2
LESIZE,1, , ,30
L,2,3
LESIZE,2, , ,35
L,3,4
LESIZE,3, , ,100,10
L,4,5
LESIZE,4, , ,75
L,5,6
L,6,7
L,7,8
L,8,9
L,9,10
LESIZE,9, , ,50
L,10,1
LESIZE,10, , ,65
L,10,11
LESIZE,11, , ,50
L,11,12
LESIZE,12, , ,50
```

Appendix 1 (Continued)

```
L,11,8
LESIZE,13, , ,100
L,12,7
LESIZE,14, , ,100
L,3,11
LESIZE,15, , ,360,20
L,4,12
LESIZE,16, , ,75

! AREAS

AL,1,2,15,11,10
AL,15,3,16,12
AL,4,5,6,14,16
AL,13,12,14,7
AL,11,13,8,9

! FIBER PROPERTIES

Efy=260E09
Efx=14E09
Efz=14E09
Vf=0.75
Vm=1-Vf
PSRfyx=0.26
PSRfxy=(PSRfyx*Efx)/Efy
PSRfyz=0.26
PSRfxz=0.33
Gfyx=51E09
Gfyz=51E09
Gfxz=8.27E09
CTEfy=-0.855E-06
CTEfx=3.24E-06
CTEfz=3.24E-06

! MATRIX PROPERTIES

Em=3.5E09
PSRm=0.35
Gm=Em/(2*(1+PSRm))
CTEm=90E-06
```

Appendix 1 (Continued)

```
! COMPOSTE FORMULAS

Eyy=Efy*Vf+Em*Vm
Exx=(Em)/(1-(Vf**0.5)*(1-Em/Efx))
Ezz=(Em)/(1-(Vf**0.5)*(1-Em/Efx))

Gyx=(Gm)/(1-(Vf**0.5)*(1-Gm/Gfyx))
Gyz=(Gm)/(1-(Vf**0.5)*(1-Gm/Gfyx))
Gxz=(Gm)/(1-(Vf**0.5)*(1-Gm/Gfxz))

PSRyx=PSRfXY*Vf+PSRm*Vm
PSRxy=(PSRyx*Exx)/Eyy
PSRyz=PSRfxy*Vf+PSRm*Vm
PSRxz=(Exx/(2*Gxz))-1

CTEyy=(Efy*CTEfy*Vf+Em*CTEm*Vm)/(Efy*Vf+Em*Vm)
CTExx=Vf*CTEfy*(1+PSRfyx)+Vm*CTEm*(1+PSRm)-
(Vf*PSRfyx+Vm*PSRm)*CTEyy
CTEZZ=Vf*CTEfy*(1+PSRfyx)+Vm*CTEm*(1+PSRm)-
(Vf*PSRfyx+Vm*PSRm)*CTEyy

! MATERIAL 1      (FIBER)

MP,EY,1,Efy
MP,EX,1,Efx
MP,EZ,1,Efz
MP,PRXY,1,PSRfXY
MP,PRYZ,1,PSRfyz
MP,PRXZ,1,PSRfxz
MP,GXY,1,GfYX
MP,GYZ,1,GfYZ
MP,GXZ,1,Gfxz
MP,ALPX,1,CTEfx
MP,ALPY,1,CTEfy
MP,ALPZ,1,CTEfz
MP,REFT,1,170

! MATERIAL 2      (MATRIX)

MP, EX, 2, Em
MP, PRXY, 2, PSRm
```

Appendix 1 (Continued)

```
MP, ALPX, 2, CTEm
MP, REFT, 2,170

! MATERIAL 3      (COMPOSITE)

MP,EX,3,Exx
MP,EY,3,Eyy
MP,EZ,3,Ezz
MP,PRXY,3,PSRXY
MP,PRYZ,3,PSRyz
MP,PRXZ,3,PSRxz
MP,GXY,3,Gyx
MP,GYZ,3,Gyz
MP,GXZ,3,Gxz
MP,ALPX,3,CTExx
MP,ALPY,3,CTEyy
MP,ALPZ,3,CTEzz
MP,REFT,3,170

BFUNIF,TEMP,20
A262=A/262
KSCON,2,A262,1,6,1

MAT,1
AMESH,1
MAT,1
AMESH,5
MAT,2
AMESH,2
MAT,2
AMESH,4
MAT,3
AMESH,3

! BOUNDARY CONDITIONS

DL,2,1,SYMM
DL,3,2,SYMM
DL,4,3,SYMM
```

Appendix 1 (Continued)

```
DL,8,5,UY,0.46587
DL,6,3,UY,0.46587
DL,7,4,UY,0.46587

Finish
/Solu
Solve
finish

NSEL,R,LOC,X,0.9999999,1.00001
NSEL,R,LOC,Y,0,30
```

Appendix 2: Maple Instructions

p : pressure on crack
a: Radius of crack
E: Young's modulus
nu: Poisson's ratio
mu: Shear modulus
rin, zin: radial and z loaction, respectively

```
> restart;
p:=-50000; a:=1.0; E:=30E6;nu:=0.3;mu:=E/(2.*(1+nu)) ;rin:=0.581468892926;
zin:=0.107101144421;

> A:=-p/(Pi*mu)*(sin(s*a)-s*a*cos(s*a))/(s^2);

> f:=int(A/s*BesselJ(0,r*s)*exp(-s*z),s=0..infinity);

> sz:=2*mu*(-diff(f,z,z)+z*diff(f,z,z,z));

> stheta:=2*mu*(1/r*diff(f,r)+2*nu*diff(f,r,r)+z/r*diff(f,r,z));

> sr:=2*mu*((1-2*nu)*diff(f,r,r)-2*nu*diff(f,z,z)+z*diff(f,r,r,z));

> trz:=2*mu*z*diff(f,r,z,z);

> ur:=(1-2*nu)*diff(f,r)+z*diff(f,r,z);

> uz:=(-2*(1-nu)*diff(f,z))+z*diff(f,z,z);

> evalf(subs(r=rin,z=zin,ur));

> evalf(subs(r=rin,z=zin,uz));

> evalf(subs(r=rin,z=zin,sr));

> evalf(subs(r=rin,z=zin,sz));
```

Appendix 2 (Continued)

```
> evalf(subs(r=rin,z=zin,stheta));

> evalf(subs(r=rin,z=zin,trz));
```

Appendix 3: Mathcad File

$r := 1.00$

$z := 0.237853902209 \cdot 10^{-1}$

$\nu := 0.3 \qquad E := 30 \cdot 10^{6} \qquad p_{nc} := 50000$

$\varepsilon_r := \frac{-\nu \cdot p_{nc}}{E} \qquad u_{r.nc} := \varepsilon_r \cdot r \qquad u_{r.nc} = -0.0005$

DISPLACEMENTS

$u_{r.c} := -0.0002309016707$ From Maple $\qquad u_{r.total} := u_{r.nc} + u_{r.c}$

$u_{r.total} = -7.30902 \times 10^{-4}$ $\qquad u_{r.ansys} := -0.72998 \cdot 10^{-3}$ From Ansys

$\varepsilon_{ur} := \left| \left(\frac{u_{r.total} - u_{r.ansys}}{u_{r.total}} \right) \cdot 100 \right| \qquad \varepsilon_{ur} = 0.126$

$\varepsilon_z := \frac{p_{nc}}{E} \qquad u_{z.nc} := \varepsilon_z \cdot z \qquad u_{z.nc} = 0.000039642317$

$u_{z.c} := 0.00002240994425$ From Maple $\qquad u_{z.total} := u_{z.nc} + u_{z.c}$

$u_{z.total} = 0.0000621$ $\qquad u_{z.ansys} := 0.61989 \cdot 10^{-4}$ From Ansys

$\varepsilon_{uz} := \left| \left(\frac{u_{z.total} - u_{z.ansys}}{u_{z.total}} \right) \cdot 100 \right| \qquad \varepsilon_{uz} = 0.102$

STRESSES

$\sigma_{r.c} := 41963.92344$ From Maple

$\sigma_{r.nc} := 0$

$\sigma_{r.total} := \sigma_{r.c} + \sigma_{r.nc}$

$\sigma_{r.total} = 41963.9234$

$\sigma_{r.ansys} := 41950$ From Ansys

$$\varepsilon_{\sigma r} := \left| \frac{\sigma_{r.total} - \sigma_{r.ansys}}{\sigma_{r.total}} \right| \cdot 100$$

$\varepsilon_{\sigma r} = 0.033$

$\sigma_{\theta.c} := 21332.52740$ From Maple

$\sigma_{\theta.nc} := 0$

$\sigma_{\theta.total} := \sigma_{\theta.c} + \sigma_{\theta.nc}$

$\sigma_{\theta.total} = 21332.5274$

$\sigma_{\theta.ansys} := 21326$ From Ansys

$$\varepsilon_{\sigma\theta} := \left| \frac{\sigma_{\theta.total} - \sigma_{\theta.ansys}}{\sigma_{\theta.total}} \right| \cdot 100$$

$\varepsilon_{\sigma\theta} = 0.031$

$\sigma_{z.c} := 52234.66801$ From Maple

$\sigma_{z.nc} := 50000$

$\sigma_{z.total} := \sigma_{z.c} + \sigma_{z.nc}$

$\sigma_{z.total} = 102234.668$

$\sigma_{z.ansys} := 0.10214 \cdot 10^{6}$ From Ansys

$$\varepsilon_{\sigma z} := \left| \frac{\sigma_{z.total} - \sigma_{z.ansys}}{\sigma_{z.total}} \right| \cdot 100$$

$\varepsilon_{\sigma z} = 0.093$

$\sigma_{rz.c} := 11742.67654$ From Maple

$\sigma_{rz.nc} := 0$

$\sigma_{rz.total} := \sigma_{rz.c} + \sigma_{rz.nc}$

$\sigma_{rz.total} = 11742.6765$

$\sigma_{rz.ansys} := 11739$ From Ansys

$$\varepsilon_{\sigma rz} := \left| \frac{\sigma_{rz.total} - \sigma_{rz.ansys}}{\sigma_{rz.total}} \right| \cdot 100$$

$\varepsilon_{\sigma rz} = 0.031$